Clays and Clay Minerals, Vol. 58, No. 5, 644–666, 2010.

GEOCHEMISTRY OF MIXED-LAYER ILLITE-SMECTITES FROM AN EXTENSIONAL BASIN, ANTALYA UNIT, SOUTHWESTERN TURKEY

Ömer Bozkaya* and Hüseyin Yalçın

Department of Geological Engineering, Cumhuriyet University, TR-58140 Sivas, Turkey

Abstract—The Antalya Unit, one of the allochthonous units of the Tauride belt, is of critical, regional tectonic importance because of the presence of rifting remnants related to the break-up of the northern margin of Gondwana during Triassic time. Paleozoic–Mesozoic sedimentary rocks of the Antalya Unit consist mainly of calcite, dolomite, quartz, feldspar, and phyllosilicate (illite-smectite, smectite, kaolinite, chlorite, illite, chlorite-smectite, and chlorite-vermiculite) minerals. Illite-smectite (I-S) was found in all of the sequences from Cambrian to Cretaceous, but smectite was only identified in Late Triassic-Cretaceous sediments. R0 I-S occurs exclusively in early-diagenetic Triassic–Cretaceous units of the Alakırçay Nappe (rift sediments), whereas R3 I-S is present in late-diagenetic to low-anchimetamorphic Cambrian–Early Triassic units of the Tahtalıdağ Nappe (pre-rift sediments). Kübler Index (KI) values and the illite content of I-S reflect increasing diagenetic grades along with increasing depth. Major-element, trace-element, rare-earth-element (*REE*), and stable-isotope (O and H) compositions were investigated in dioctahedral and trioctahedral smectites and I-S samples from the pre-rift and rift-related formations. Both total layer charge and interlayer K increase, whereas tetrahedral Si and interlayer Ca decrease from smectite to R3 I-S. Trace-element and *REE* concentrations of the I-S are greater in pre-rift sediments than in rift sediments, except for P, Eu, Ni, Cu, Zn, and Bi. On the basis of North American Shale Composite (NASC)-normalized values, the *REE* patterns of I-S in the pre-rift and rift sediments are clearly separate and distinct. Oxygen ($\delta^{18}O$) and hydrogen (δD) values relative to SMOW (Standard Mean Oceanic Water) of smectite and I-S reflect supergene conditions, with decreasing $\delta^{18}O$ but increasing δD values with increasing diagenetic grade. Lower δD values for these I-S samples are characteristic of rift sediments, and pre-rift sediments have greater values. On the basis of isotopic data from these I-S samples, the diagenesis of the Antalya Unit possibly occurred under a high geothermal gradient (>35ºC/km), perhaps originating under typical extensional-basin conditions with high heat flow. The geochemical findings from I-S and smectites were controlled by diagenetic grade and can be used as an additional tool for understanding the basin maturity along with mineralogical data.

Key Words—I-S Mineralogy, Major Elements, O-H Isotopes, Trace Elements.

INTRODUCTION

Extensional basins show increasing diagenetic- to low-grade metamorphic characteristics with depth, and have counterclockwise pressure-temperature-time (*P-T-t*) trajectories – initially with increasing temperature during extension, and subsequently by increasing pressure during basin inversion (*e.g.* Robinson, 1987; Robinson and Bevins, 1986). Temperature is an important factor in certain types of basins because of their greater heat flow and geothermal gradient (35ºC/km) relative to passive marginal basins with smaller geothermal gradients (25–30ºC/km) (*e.g.* Merriman and Peacor, 1999; Merriman, 2005). Phyllosilicate reaction processes that convert smectite to illite yield mixed-layer illite-smectite (I-S) phases, which are randomly interstratified (R0 type) at smaller illite contents and then become ordered (R3 type) at greater illite contents. During this transformation, the interlayer K and tetrahedral layer charge increase due to Al substitution for Si, and the octahedral layer charge increases because of Fe(II) and Mg substitution for Al. Such mineralogical and geochemical changes are, in many cases, encountered in clay-rich sediments during burial diagenesis/metamorphism, as has been well documented in studies over the last 30 y (*e.g.* Hower *et al*., 1976; Velde *et al*., 1986; Merriman and Frey, 1999; Merriman and Peacor, 1999; Abid *et al*., 2004). On the other hand, the trace- and, in particular, rare earth element (*REE*) compositions of clay minerals have been used in many cases to establish sedimentary process(es) and provenance (Fleet, 1984; McLennan, 1989; Condie, 1991), and to evaluate diagenetic/metamorphic grades (Milodowski and Zalaciewicz, 1991; Ohr *et al*., 1994). Moreover, stable-isotopic (O and H) compositions of illitic clays from sedimentary environments may reflect some thermal events during diagenetic/metamorphic processes (*e.g.* Savin and Lee, 1988; Sheppard and Gilg, 1996).

In this context, I-S is considered to be a prime regulator of a wide variety of diagenetic and chemical processes, and indications of the origin and behavior of their chemical compositions might indirectly be of more

* E-mail address of corresponding author:
bozkaya@cumhuriyet.edu.tr
DOI: 10.1346/CCMN.2010.0580505

general interest and help to solve questions with regard to using these minerals as tectonic indicators and recorders of the burial evolution of sedimentary basins. However, a paucity of information exists on relationships between I-S ordering and their geochemistry in extensional basins. The present study focused, therefore, on the Antalya Unit, an allochthonous body of strata from the Tauride-Anatolide Platform or Tauride-Anatolide Composite Terrane (TACT; Göncüoğlu *et al.*, 1997), a continental microplate comprising several tectonostratigraphic units deposited during the Phanerozoic, including remnants of Triassic rifting (Robertson and Woodcock, 1981), and shows typical extensional basin characteristics (Bozkaya and Yalçın, 2005). It also represents a critical part of the evidence for a southerly Neotethyan oceanic basin in the easternmost Mediterranean region, and offers evidence for rifting of the Neotethys in the Late Permian–Middle Triassic related to the break-up of the northern margin of Gondwana prior to spreading from the mid-Triassic onwards (Robertson, 1994).

In addition to previous studies of the stratigraphic-sedimentological framework of the Kemer-Kumluca area (Robertson and Woodcock, 1981; Robertson, 1994), some mineralogical monitoring was also presented for the eastern extension of the Antalya Unit in the Alanya-Gazipaşa area (Bozkaya and Yalçın, 2005). The mineralogical and geochemical characteristics of illitic clays in the Cambrian–Cretaceous sequence of the Kemer-Kumluca area are unknown; in this area, exposures constitute the type area, and all of the main units are well exposed. The present study was designed to elucidate the diagenetic/metamorphic characteristics of these clays and to explain the mineralogical and geochemical differences of clays in response to basin maturation during pre-rift and rift-related events.

GEOLOGIC SETTING

Regional geology

The study focuses on the Antalya Unit of the western Tauride Belt in the southwestern part of Turkey (Figure 1), which is exposed in segments in the Isparta and Demirtaş-Alanya areas (Bozkaya and Yalçın, 2005); exposures in the Kemer-Kumluca area, comprising Cambrian—Cretaceous units, are well known and constitute the type sections.

The Tauride Belt, which was located on the northern marginal platform of Gondwana until the Early Mesozoic opening of the southern Neotethyan oceanic seaway (*e.g.* Şengör and Yılmaz, 1981), forms an alpine unit including numerous nappes or tectonostratigraphic units (Özgül, 1976) that were formed during the closure of the Neotethyan oceans (Figure 1a). Of these, the Geyikdağı Unit includes Precambrian to Tertiary sedimentary and metasedimentary rocks, and records mainly increasing diagenetic/metamorphic grade with increasing depth or age (Bozkaya and Yalçın, 2004a; Bozkaya *et al.*, 2002, 2006). The Bozkır Unit, the uppermost tectonic unit of the allochthonous nappe pile, consists mainly of Mesozoic slope to passive margin deposits. The Aladağ and Bolkardağı units have the lowermost successions of Devonian age and also a very low-grade metamorphic character related to extensional-basin conditions (Bozkaya and Yalçın, 2004a). The Alanya Unit comprises three Paleozoic–Early Mesozoic metamorphic nappes (Mahmutlar, Sugözü, and Yumrudağ), and each has a different source and metamorphic properties (Bozkaya and Yalçın, 2004b). Cambrian–Cretaceous sedimentary-metasedimentary lithologies of the Antalya Unit crop out in both the central and western parts of the Tauride Belt, and also locally in the western Tauride Belt around Kemer and Kumluca.

In the study area, the Antalya Unit is tectonically underlain by the Beydaglari Autochthon of the Geyikdagi Unit, and has been thrusted over by the Tekirova ophiolite nappes (Figure 1b). It comprises several tectonostratigraphic units, namely the Çataltepe, Alakırçay, and Tahtalıdağ nappes (Şenel, 1997; Şenel *et al.*, 1998). The first nappe, described as the lower nappe (Brunn *et al.*, 1971; Dumont *et al.*, 1972), comprises Norian-Upper Maastrichtian sedimentary rocks deposited under platform and slope-basinal conditions. The second nappe, known as the middle nappe (Brunn *et al.*, 1971; Dumont *et al.*, 1972) or Kumluca zone (Robertson and Woodcock, 1981), is made up of rift-related Triassic–Early Cretaceous clastic, carbonate, and volcanic-volcanosedimentary rocks, which typically comprise continental fragments of a spreading-ridge-type tectonic setting, suggesting only limited subsidence and including preserved fragments of continental crust (Robertson, 1994). Upper Triassic alkaline lavas interbedded with pelagic sediments are widespread, however, and the presence of Jurassic–Early Cretaceous alkaline lavas was also determined in this unit (Yılmaz, 1984), suggesting the possibility of an oceanic protolith existing from the Late Triassic to Late Cretaceous. The third nappe, or Kemer zone (Robertson and Woodcock, 1981), interpreted as the upper nappe that was transported large distances (Brunn *et al.*, 1971; Dumont *et al.*, 1972), comprises mainly pre-rift sedimentary rocks deposited during the Cambrian-Triassic time interval. In the present study, the Tahtalıdağ and Alakırçay nappes were investigated because of corresponding pre-rift and rift-related sediments, respectively.

Stratigraphy and lithology

The pre-rift (Tahtalıdağ nappe or Kemer zone) and rift-related formations (Alakırçay nappe or Kumluca zone) of the Antalya Unit include different rock units with respect to age and tectonic setting (Figure 2). In the study area, the Tahtalıdağ nappe is dominated by steeply dipping slices of Paleozoic (Cambrian to Permian) sedimentary rocks. The lowermost parts of the

https://doi.org/10.1346/CCMN.2010.0580505 Published online by Cambridge University Press

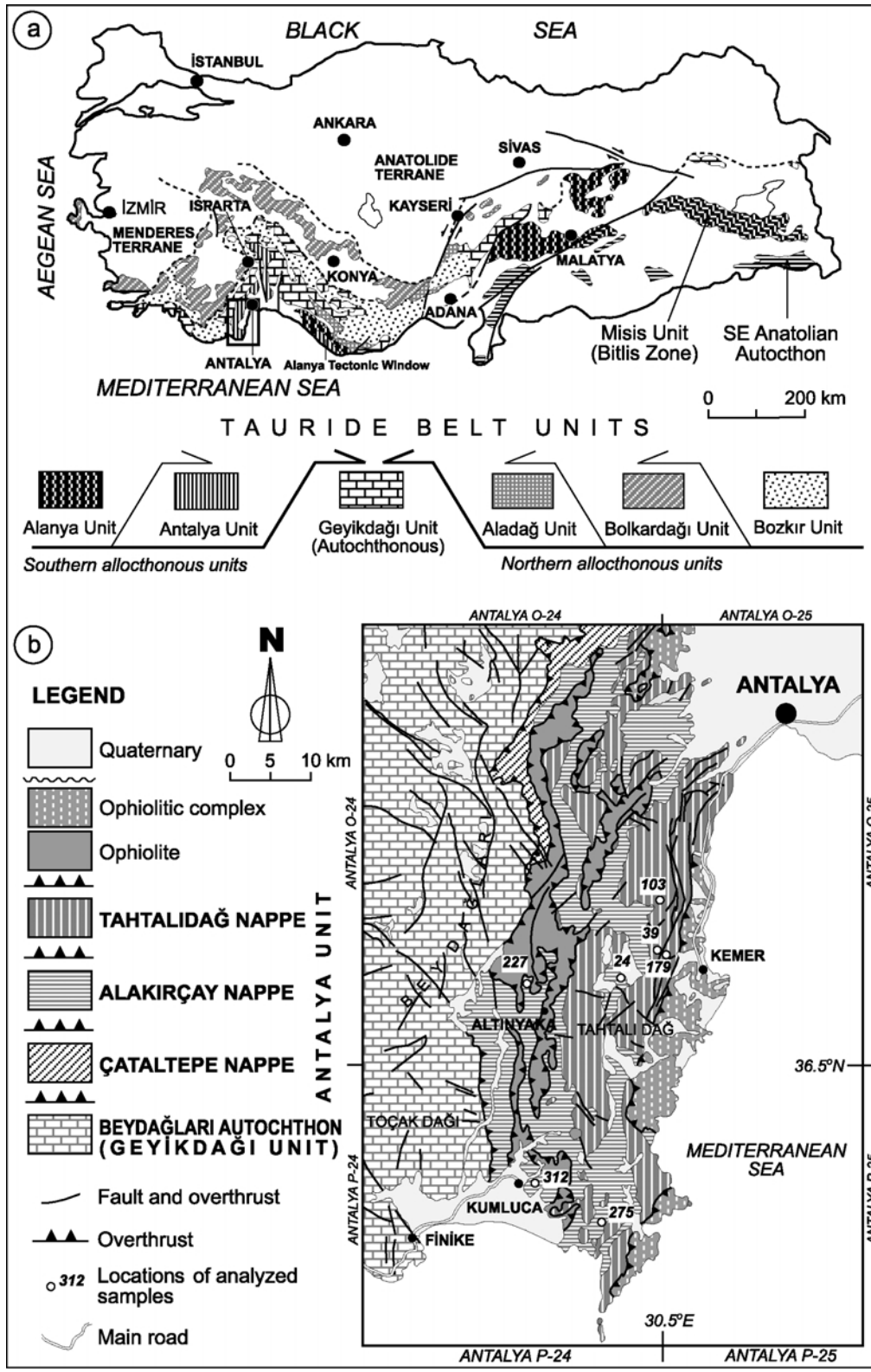

Figure 1. (a) Tectonic map of southern Turkey showing the major Alpine units with Paleozoic rock units (Özgül, 1976); (b) regional geological map of the western Taurides with geographic distributions of the nappes of the Antalya Unit (Şenel, 1997), and the locations of samples used for geochemical analysis.

https://doi.org/10.1346/CCMN.2010.0580505 Published online by Cambridge University Press

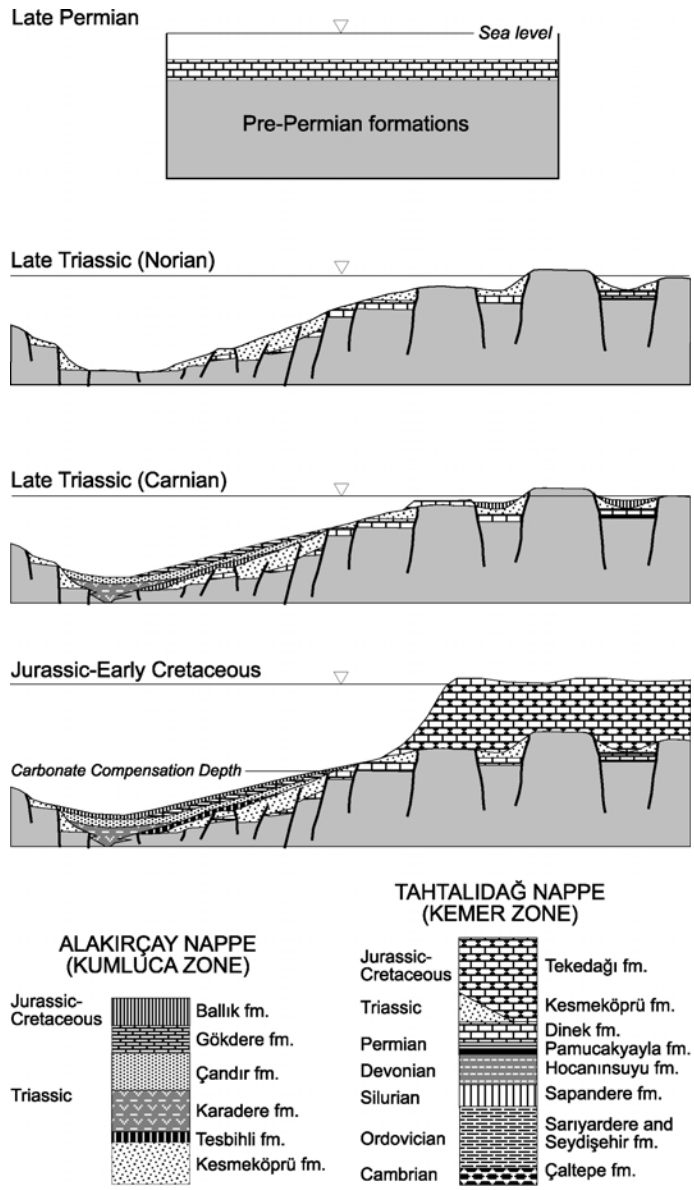

Figure 2. Stratigraphic construction and vertical distribution of pre-rift and rift-related formations from Antalya Unit (modified from Robertson and Woodcock, 1981).

Tahtalıdağ nappe comprise Middle Cambrian recrystallized nodular limestones and dolomites; silica and barite veins of the Çal Tepe formation that is followed by the Upper Cambrian–Lower Ordovician Seydişehir formation, with its grayish-brown slates and metasandstone alternations; and the Upper Ordovician Sarıyardere formation, containing grayish-brown metashales and/or slates with metasiltstone and metasandstone intercalations. The Silurian Sapandere formation rests along a regional unconformity on the Ordovician sequence, comprising sandstone, shale, limestone, and scarce dolomite, and is overlain conformably by the Sarıyardere formation. Both are overlain along an angular unconformity by the Devonian Hocanınsuyu formation, comprising limestone, dolomite, sandstone, siltstone, and shale lithologies. The Devonian angular unconformity on the older units is a characteristic event in the Antalya, Geyikdağı, and Alanya units of the Tauride Belt, and it constitutes the main difference between the northern and southern units (Göncüoğlu and Kozlu, 2000). The Upper Permian Pamucakyayla formation is made up of mainly grayish-black shale with intercalated sandstone and coal measures. The Upper Permian Dinek formation comprises fossiliferous limestone and dolomite with shale laminations. The unit consists of Upper Triassic-Cretaceous shallow-water

https://doi.org/10.1346/CCMN.2010.0580505 Published online by Cambridge University Press

carbonate rocks overlying Paleozoic sequences, which lack rifted areas (Figure 2).

The Alakırçay nappe typically comprises rift-related formations deposited within an extensional basin, mainly thrust-imbricated deep-water passive margin sediments of Triassic-Cretaceous age (Kalafatçıoglu, 1973; Şenel (1997). The lowest part of the nappe is the Early–Middle Triassic (Scitian–Anisian) Kesmeköprü formation, comprising multicolored clayey-calcareous rocks such as shale and marl, with scarce gypsum. The Jurassic–Cretaceous Tekedağı formation comprises platform-type carbonate rocks, >1000 m thick. The Middle Triassic (Late Ladinian−Early Carnian) Tesbihli formation comprises chiefly brown−claret red, thin- to medium-bedded radiolarite, chert, and siliceous-shale alternations (Şenel, 1997). The Late Triassic (Ladinian–Norian) Karadere formation is made up mainly of volcanogenic rocks, namely basaltic pillow lavas, spilitic basalt with carbonate, and zeolite amygdales, agglomerate, and tuff. Late Carnian radiolarian and conodont faunas were determined in the associated sediments within submarine lavas, consisting of within-plate-type alkaline basalts characterized by a multi-element pattern similar to typical oceanic-island basalts (Varol *et al.*, 2007; Maury *et al.*, 2008). The Middle–Late Triassic (Early Anisian-Norian) Çandır formation comprises green, claret-red, and gray sandstone-shale alternations, and scarce radiolarite, chert, and tuff. The Late Triassic (Carnian−Rhaetian) Gökdere formation consists of beige−gray chert-nodule-bearing-fossiliferous limestone with Early to Middle Norian radiolarians (Tekin and Yurtsever, 2003) and chalk-like marl; locally, bedded chert, tuff, and pillow lavas are also present. The uppermost formation of the Alakırçay nappe is the Jurassic−Cretaceous Ballık formation; it comprises bedded radiolarite-chert and siliceous claystone and tuff lithologies. Lower Jurassic (Hettangian–Sinemurian) radiolarians were identified within thin-bedded limestone beds at the base of the formation (Tekin, 2002). The presence of alkaline lava was also reported in the Jurassic−Cretaceous unit, along with the presence of tuffs and radiolarite-bearing lithologies (Yılmaz, 1984).

MATERIAL AND METHODS

A total of 277 samples collected from measured stratigraphic sections, avoiding hydrothermal zones and main tectonic lines, were studied in thin section using a polarizing microscope, by scanning electron microscopy (SEM) with energy dispersive spectrometry (EDS), by X-ray diffractometry (XRD), and by chemical analyses covering major-, trace-, and rare-earth elements (*REE*) and stable isotopes (O-H).

Textural and mineralogical features of metaclastic-rock samples were examined by transmitted light microscopy. In addition, gold- and carbon-coated fragments were examined by SEM with a JEOL JSM-6490 instrument at the Turkish Petroleum Corporation in Ankara, Turkey, in order to obtain textural, morphological, and chemical information from mineral phases in these rocks. Operating conditions were 32 s counting time and 20 kV accelerating voltage.

The XRD analyses were performed using a Rigaku DMAX IIIC X-ray diffractometer in the Department of Geological Engineering of Cumhuriyet University (Sivas, Turkey). Samples were analyzed using Cu-Kα (1.541871 Å) radiation with a Ni filter or a diffracted-beam monochromator, accelerating voltage of 35 kV, beam current of 20 mA, divergence slit = 1º, scatter slit = 1º, receiving slit = 0.3 mm, monochromator receiving slit = 0.8 mm, and scan speeds of 2º2θ/min and 1º2θ/min in the range 5−35º2θ and 2−30º2θ for whole-rock and oriented clay fractions, respectively. The results obtained constitute semi-quantitative analyses using the external standard method of Brindley (1980).

The clay fractions (<2 μm) for mineralogical investigations were separated by centrifugation after dispersion. The samples were ground slightly prior to clay extraction in order to prevent clastic micas from entering the clay-sized fraction. The peptizing components (carbonates and organic matter) were eliminated *via* acid treatment of the samples. The oriented samples of clay minerals were prepared by pipetting the clay suspension and/or smearing the clay mud onto glass slides. The mineralogical compositions of the clay fractions were assessed by XRD. For these analyses, samples of specific fractions were solvated with ethylene glycol (EG) at 60ºC for 16 h, and subsequently heated to 490ºC for 4 h.

Illite 'crystallinity' indices, also known as the Kübler indices (KI: Kübler, 1968; Guggenheim *et al.*, 2002), were determined by measuring the width at half height, Δº2θ, of the 001 illite reflection of air-dried and glycolated samples. The KI values were calibrated both to Kisch's scale (Kisch, 1980, 1991a) and to the CIS scale (Warr and Rice, 1994).

The illite and smectite ratios in I-S were obtained from calculated patterns using the *NEWMOD* software program (Reynolds, 1985). Furthermore, the different interstratification types in these minerals were distinguished using the *WINFIT* software program (Krumm, 1996), which reconstructed single peaks by fitting the envelope curve of overlapping peaks.

Pure and nearly pure I-S and smectite fractions for chemical analysis were extractable only from seven samples (Table 1). The chemical compositions and the hydrogen- and oxygen-isotopic compositions of these clay fractions were determined using a Thermo Jarrell-Ash ENVIRO II ICP, a Varian Vista 735 inductively coupled plasma (ICP) spectrometer, a Perkin-Elmer SCIEX ELAN Model 6000, 6100, or 9000 inductively coupled plasma-mass spectrometer (ICP-MS), or a Finnigan MAT 250 mass spectrometer at the ACTLABS Activation Laboratory, Ltd. (Ancaster, Ontario, Canada).

https://doi.org/10.1346/CCMN.2010.0580505 Published online by Cambridge University Press

Table 1. Some mineralogical properties of the samples analyzed.

Sample no.	Formation (age)	Lithology (diagenetic grade)	Mineralogy			
			Bulk	Clay	d_{060} (Å)	Polytype
TAK-227	Ballık (Jurassic-Cretaceous)	Siliceous ash tuff (early diagenesis)	Phl+Qtz	S ± K	1.499	–
TAK-275	Karadere (Triassic)	Volcanic claystone (early diagenesis)	Phl	S	1.527	–
TAK-312	Gökdere (Triassic)	Clayey limestone (early diagenesis)	Cal+Phl+Qtz	I-S	1.501	–
TAK-24	Çandır (Triassic)	Shale (late diagenesis)	Phl+Qtz+Cal+Fel	I-S	1.502	–
TAK-179	Kesmeköprü (Triassic)	Clayey limestone (late diagenesis)	Cal+Phl+Qtz	I-S ± I	1.503	$1M_d$
TAK-39	Hocanınsuyu (Devonian)	Mudstone (late diagenesis)	Qtz+Phl+Fel+Cal	I-S	1.503	$1M+1M_d$
TAK-103	Sapandere (Silurian)	Clayey sandstone (late diagenesis)	Qtz+Phl+Fel	I-S	1.505	$1M+1M_d$

Phl: phyllosilicate, Qtz: quartz, Cal: calcite, Fel: feldspar, S: smectite, K: kaolinite, I-S: illite-smectite, I: illite.

Samples were prepared and analyzed in a batch system for oxides and trace elements, mixed with a flux of lithium metaborate/tetraborate, and fused in an induction furnace. The melt was immediately poured into a solution of 5% HNO_3 containing an internal standard and mixed continuously until completely dissolved (~30 min).

For analysis of $^{18}O/^{16}O$ isotopic ratios, samples were reacted with BrF_5 at ~650ºC in nickel bombs following the procedures described by Clayton and Mayeda (1963). The fluorination reaction converts O in the minerals to O_2 gas, which is subsequently converted to CO_2 gas using a hot C rod. For D/H isotope ratios, samples weighing 0.02 to 1.0 g were wrapped in molybdenum foil and placed in a platinum crucible, which was then suspended inside a quartz extraction vessel. The vessel and its contents were outgassed in a vacuum at 120ºC for 4 h to remove surface-adsorbed water. The sample was then heated inductively at 1400ºC for up to 20 min and the gases collected in a trap held at −196ºC. Nearly all of the hydrogen was thus released in the form of water, but miniscule quantities of hydrocarbons or molecular hydrogen released or produced during this treatment were oxidized over CuO at 550ºC to form H_2O and CO_2, which were also collected in the trap. The accumulated water – representing the total amount of hydrogen in the samples – was separated from the other gases by differential freezing techniques. The water was reacted with uranium at 900ºC to produce H_2 and collected on charcoal at −196ºC. The O-H isotopic data are reported in the standard delta notation as per mil deviations from V-SMOW.

PETROGRAPHY

Optical microscopy

Metaclastic rocks of the Ordovician Seydişehir formation are characterized by distinctive bedding orientations and poorly developed cleavage planes (Figure 3a). The presence of biotite-muscovite and chlorite-muscovite stacks and the chloritization of biotite are typical features of this unit. Quartz and plagioclase boundaries are sutured with sericitized and chloritized groundmass. Chloritization of biotite and chlorite-mica stacks indicate that detrital biotite is of volcanic provenance and was altered under very low-grade metamorphic conditions (*e.g.* Kisch, 1991b; Merriman, 2005). Metaclastic rocks of the Ordovician Sarıyardere formation are characterized by relatively poor cleavage development. Silurian and younger units have no metamorphic textures and are characterized solely by primary diagenetic properties. The sandstones of the Sapandere, Hocanınsuyu, and Pamucakyayla formations are subarkose and quartz arenite in composition, and in these rocks the presence of monocrystalline and polycrystalline quartz and microcline fragments together with polysynthetically twinned plagioclase

https://doi.org/10.1346/CCMN.2010.0580505 Published online by Cambridge University Press

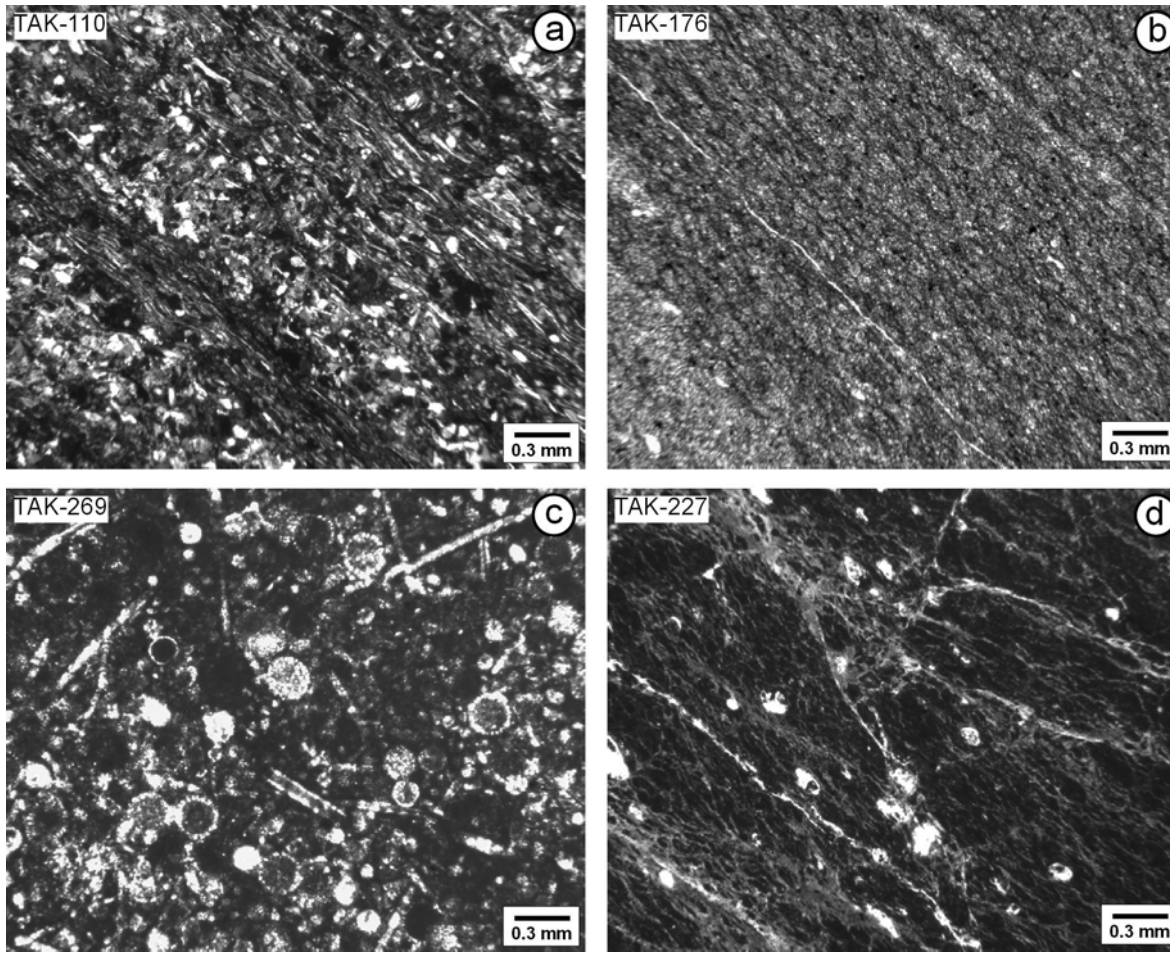

Figure 3. Optical photomicrographs of samples from the Antalya Unit. (a) Microlaminations and distinct orientation of metasiltstone from the Seydişehir formation (crossed nicols); (b) orientation and partial recrystallization of micritic limestones from the Kesmeköprü formation (plane polarized light); (c) well preserved radiolarian fossils and sponge spicules within the Fe oxide and clay matrix of radiolarite from the Çandır formation (plane polarized light); (d) silicified radiolarite and silica veins within the argillized ash tuff from Ballık formation (plane polarized light).

indicate a granitoid provenance during Silurian–Permian time. Detrital micas are generally not observed or are scarce in sandy and silty lithologies; therefore, the phyllosilicates were authigenic or transformed from the clay matrix. Authigenic kaolinite and scarce ellipsoidal glauconite occurrences were also found in addition to I-S within the micropores of Pamucakyayla formation sandstone. Carbonate rocks of the Dinek formation include fossils (*Mizzia* sp.) and intraclasts of allochems that are classified as biomicrosparite, biomicrite, biomicrosparite, dolomitic microsparite, and dolomitic biosparite (Folk, 1968). Locally, carbonate rocks occur with stylolitic texture. The Triassic Kesmeköprü formation comprises mainly micritic/microsparitic limestones (fossiliferous micrite, dolomitic microsparite) having relatively widespread recrystallization texture (Figure 3b). Marl samples contain clay-rich and calcareous microlaminations.

Siliceous rocks of the rift-related formations include radiolarite and cherty radiolarite. Radiolaria fossils largely preserve their original textures, but locally radiolarites are transformed into chalcedonic quartz within fine-grained silica and Fe-oxidized matrix (Figure 3c).

Sandstones of the Çandır formation – feldspathic litharenite, subarkose, and sublitharenite in composition (Folk, 1968) – typically consist of quartz, plagioclase, perthite, orthoclase with graphic texture, and rock fragments (basalt, slate, phyllite, and chert) within carbonate cement and sericitized clay matrix. Siliceous ash tuffs of the Ballık formation have vitrophyric texture, in which volcanogenic materials have been completely transformed to clay and silica (Figure 3d). Volcanic-volcanosedimentary rocks of the Karadere formation contain silicate (analcime, chlorite, C-S, tetranatrolite, hydroxyapophyllite), carbonate (calcite),

https://doi.org/10.1346/CCMN.2010.0580505 Published online by Cambridge University Press

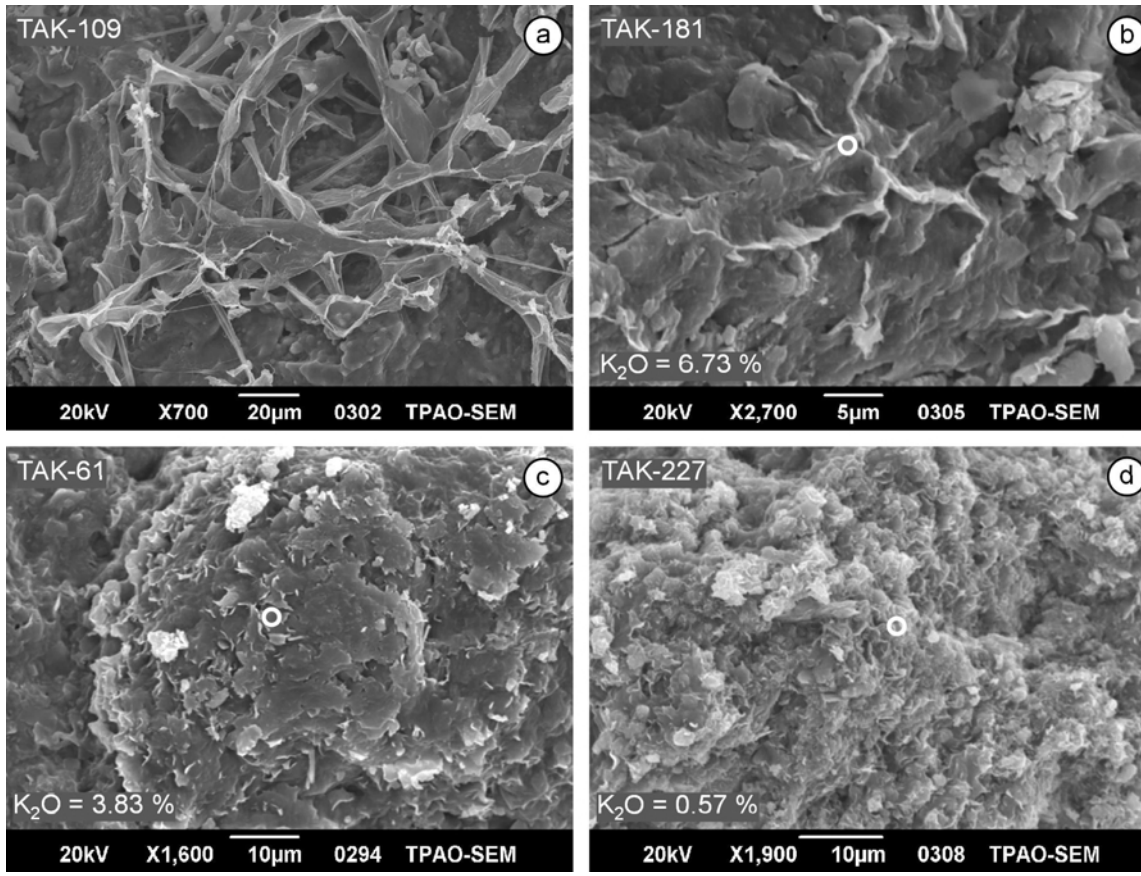

Figure 4. SEM images of I-S and smectites in clayey rocks from the Antalya Unit (wt.% values shown in the bottom left corner of images b–d reflect the EDS analytical results from analyses carried out at the location indicated by the open circle in those images). (a) Filament morphology of R3 I-S with 6.73 wt.% K_2O, from the Seydişehir formation; (b) thin, sheet-like morphology of R1 I-S with a relatively small K_2O content (3.83 wt.%), from the Kesmeköprü formation; (c) curved flakes or sheets of R0 I-S from the Gökdere formation; and (d) flaky morphology of dioctahedral smectites from the Ballık formation.

and Fe (oxyhydr)oxide (hematite, goethite) minerals within amygdales and matrix.

Scanning electron microscopy

The SEM investigations were performed on samples containing smectite and I-S (with different ordering types) in order to elucidate the relationships between textural and chemical characteristics. Crystal morphologies (*e.g.* Sudo *et al.*, 1981; Welton, 1984; O'Brien and Slatt, 1990) and semi-quantitative chemical compositions of smectite and I-S reveal differences in diagenetic grade and I-S ordering type. R3 and R1 I-S are observed as filaments and very thin sheets, respectively (Figure 4a,b), but together with a large smectite content. R0 I-S has curved flakes (Figure 4c) similar to the flaky morphology of smectite (Figure 4d). The K_2O contents of I-S and smectite obtained *via* EDS analysis yield different values for different morphologies, with greater values for filaments and thin sheets, and smaller values for flaky morphologies.

X-RAY DIFFRACTION

Bulk and clay mineralogy

The Tahtalıdağ and Alakırçay nappes are made up mainly of calcite, dolomite, quartz, plagioclase, and phyllosilicate minerals, the latter represented by mixed-layered illite-smectite (I-S), illite, kaolinite, chlorite, chlorite-smectite (C-S), chlorite-vermiculite (C-V), illite-chlorite (I-C), pyrophyllite, and smectite. In addition to these minerals, minor amounts of jarosite, hematite, goethite, gypsum, barite, siderite, analcime, tetranatrolite, and hydroxyapophyllite were also identified in the rock samples studied.

According to the average proportions of minerals (Table 2), dolomite was only detected in the Cambrian Çal Tepe and the Devonian Hocanınsuyu formations, whereas the amounts of calcite increased in the Silurian Sapandere, the Permian Dinek, and the Triassic Kesmeköprü and Gökdere formations. Quartz contents increased in the Devonian Hocanınsuyu, Permian Pamucakyayla, Triassic Tesbihli and Çandır, and

https://doi.org/10.1346/CCMN.2010.0580505 Published online by Cambridge University Press

Table 2. Mineralogic composition of pre-rift and rift-related formations (wt.%).

Age	Formation	Unit	*n*	Whole rock						Clay fraction					
				Cal	Dol	Qtz	Fel	Phl	Zeo	Fm	I	Chl	Kao	C-S	C-V	I-C	I-S	Sm
Jurassic-Cret.	Ballık	Syn-rift formations	28	7		55		38			19	5	2	3			19	52
	Gökdere		14	70		13		17			24	2					74	
	Çandır		43	21		43	8	28			31	18	5	3			31	12
Triassic	Karadere		31	10		5	24	36	17	8	12	20		25	1	1	22	19
	Tesbihli		14			67	4	29			20	1					79	
	Kesmeköprü		15	42	6	12	5	35			34	6	3				55	2
Permian	Dinek	Pre-rift formations	21	65	9	6	1	19			24	1	7				68	
	Pamucakyayla		21	2	1	43	12	39		3	12	5	17				66	
Devonian	Hocanınsuyu		29	4	7	52	11	24		1	10	16	11	1	1		61	
Silurian	Sapandere		24	28	9	27	12	24			13	5		7			75	
	Sarıyardere		16	5		23	20	51		1	20	10	13	14	3	1	39	
Ordovician	Seydişehir		14	3		38	19	40			26	13	13				48	
Cambrian	Çaltepe		4		51	42		7			65						35	

n: sample number, Cal: calcite, Dol: dolomite, Qtz: quartz, Fel: feldspar, Phl: phyllosilicate, Zeo: zeolite, Fm: ferrous minerals, I: illite, Chl: chlorite, Kao: kaolinite, C-S: chlorite-smectite, C-V: chlorite-vermiculite, I-C: illite-chlorite, I-S: illite-smectite, Sm: smectite.

Jurassic-Cretaceous Ballık formations. Feldspars are relatively abundant in the Ordovician Seydişehir and Sarıyardere, and Triassic Karadere formations. Phyllosilicate minerals abound in the Ordovician Sarıyardere, the Permian Pamucakyayla, the Triassic Kesmeköprü and Karadere, and the Jurassic–Cretaceous Ballık formations.

The I-S minerals occur in greater amounts in the clay fractions of the Cambrian to Cretaceous rocks, particularly in the Silurian–Permian Sapandere, Hocanınsuyu, Pamucakyayla, and Dinek formations. Kaolinite is present in the Ordovician Seydişehir and Sarıyardere and the Devonian–Permian Hocanınsuyu and Pamucakyayla formations. Increasing amounts of kaolinite in the Pamucakyayla formation are due to particular environmental characteristics, with low-pH conditions accompanying coal occurrences. Chlorite was determined in the Ordovician Seydişehir and Sarıyardere and the Devonian Hocanınsuyu formations, whereas C-S and C-V were found in only the Ordovician Sarıyardere and Silurian Sapandere formations. The feldspar content increases together with chlorite, C-S, and C-V in the Ordovician formations. Zeolite minerals (analcime, tetranatrolite) and hydroxyapophyllite were only detected within the amygdales in volcanogenic lithologies (pillow lava, spilitic basalt, and tuff) of the Triassic Karadere formation, having formed as a result of interaction between sea water and volcanic material. In general, diagenetic kaolinite is abundant in sandy lithologies, but I-S is more plentiful in clayey and calcareous rocks.

Discrete smectite in the I-S decreases toward the older units, as smectite → R0 + R1 I-S → R1 + R3 I-S → R3 I-S (Figure 5). *NEWMOD*®-calculated patterns and *WINFIT* peak decompositions of I-S demonstrated the presence of both R0 + R1 and R1 + R3 ordering types (Figure 6a,b). The illite proportions of the decomposed peaks of R1 and R3 I-S were calculated from the equation [illite % = 183.41 × ln ($\Delta^{o}2\theta$) − 297.48 (R^2 = 0.9896)] obtained from the data of Moore and Reynolds (1997). The illite ratios of I-S showed similar values for the Cambrian to Silurian formations, but decrease slightly in the Devonian to Triassic formations. R0 and R1 I-S are found in the Alakırçay nappe, and the illite content of I-S has smaller values in the Jurassic–Cretaceous rocks. The presence of smectite and R0 I-S is characteristic of the formations of the Alakırçay nappe. R1 I-S in the Triassic formations and R0 I-S in the Jurassic-Cretaceous Ballık formation are known, suggesting that the diagenetic grade of the Triassic units is greater than that of the Jurassic–Cretaceous unit.

Crystallinity and b-cell dimensions of illite and I-S

Kübler index values were obtained from full width at half maximum (FWHM) results of decomposed peaks from XRD patterns in which illite peaks could be separated from I-S peaks. Because of the asymmetrical

https://doi.org/10.1346/CCMN.2010.0580505 Published online by Cambridge University Press

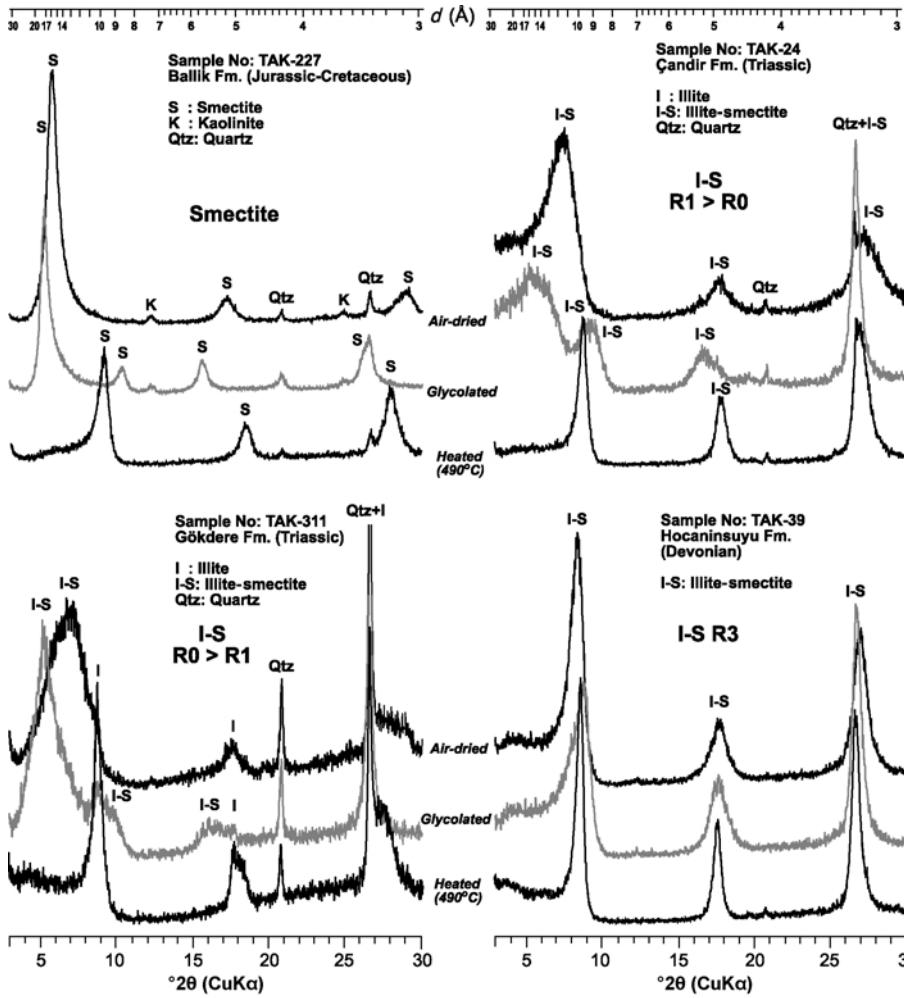

Figure 5. XRD patterns of smectite and I-S minerals from the Antalya Unit.

nature of illite peaks in the presence of I-S, KI values were measured from the symmetric extension of illite peaks, as reflected from the right sides of the peaks to their left sides (Figure 7). The KI values (0.37–0.51Δ°2θ) of the Cambrian–Silurian formations reflect low anchimetamorphic-late diagenetic grades, but greater values (0.46–0.74Δ°2θ) were determined in the Devonian–Triassic formations, indicating late- to early-diagenetic grades (Table 3). The Devonian–Triassic formations, from the Hocanınsuyu to Kesmeköprü formations, reflect late-diagenetic conditions, whereas Triassic–Cretaceous rift-related formations reflect early-diagenetic conditions. In general, the diagenetic/metamorphic grade increases from the Triassic to Cambrian units, together with increasing age and depth.

The mean *b*-cell dimension values of the illites show greater values (9.009–9.015 Å) for the Tahtalıdağ nappe (pre-rift formations) than for those (8.998–9.015 Å) of the Alakırçay nappe (rift-related formations) lithologies. Smaller *b* values are accompanied by smaller degrees of crystallinity and a smaller illite content in I-S (Table 3). Based on the *b* values of the smectites, namely, 1.499 and 1.527 Å, the Ballık and Karadere formations have dioctahedral and trioctahedral compositions, respectively.

GEOCHEMISTRY

Major-element compositions and structural formulae

Chemical and unit-cell compositions of smectite and I-S (Table 4) enabled calculation of the structural formulae of smectite and I-S on the basis of 22 negative charges corresponding to 10 oxide and two hydroxide ions (Weaver and Pollard, 1973), and the end-member muscovite composition was excluded from smectite-rich fractions because of inclusion of minor amounts (<5%) of the illite component. In this state, K_2O and related Al_2O_3, SiO_2, and H_2O equal values (1:3:6:2 for K_2O:Al_2O_3:SiO_2:H_2O, respectively) derived from the results of chemical analyses. According to vertical

https://doi.org/10.1346/CCMN.2010.0580505 Published online by Cambridge University Press

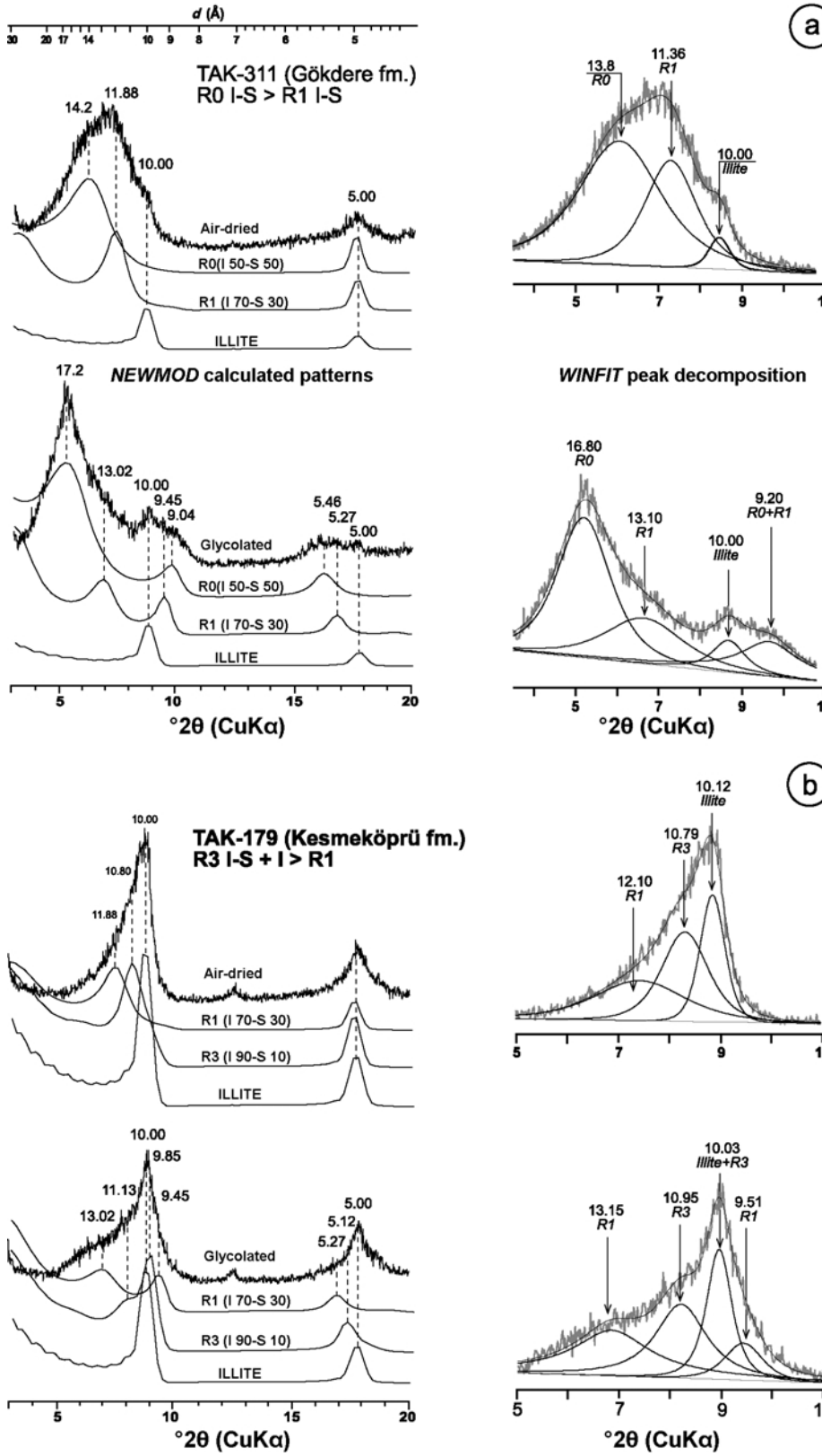

Figure 6. *NEWMOD*® calculated patterns and *WINFIT* decomposition of I-S peaks. (a) R0 and R1; (b) R1 and R3.

https://doi.org/10.1346/CCMN.2010.0580505 Published online by Cambridge University Press

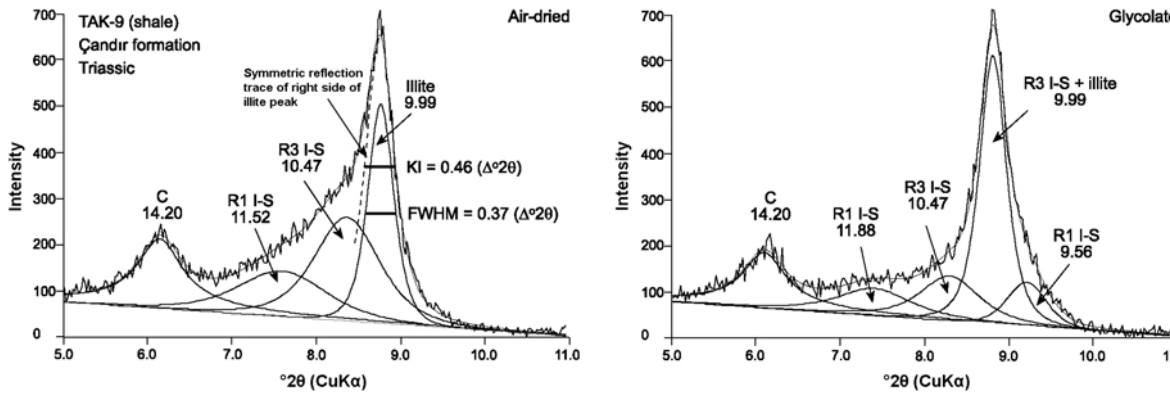

Figure 7. Peak decomposition of illite + R1 I-S + R2 I-S and chlorite reflections and KI values of illites obtained from an unresolved 10 Å peak by assuming symmetrical reflection of the right side of the peak.

distributions of major-element concentrations in the stratigraphic sequence, from R3 I-S to smectite, SiO_2 and CaO (wt.%) increase, but other oxides show no difference.

The I-S, having dioctahedral composition in many cases, have tetrahedral substitutions of 0.18 to 0.41 atoms of Al for Si per formula unit (a.p.f.u.), and octahedral substitutions of 0.17 to 0.35 atoms of Fe and 0.16 to 0.37 atoms of Mg for Al (Table 4). The total number of octahedral cations, Al, and Ti are 1.91–2.00, 1.30–1.65, and 0.02–0.06 a.p.f.u., respectively. The major interlayer cation is K (0.19–0.63 a.p.f.u.). Based on the theoretical muscovite composition (the a.p.f.u. of interlayer K = 1 and octahedral Al = 2), the numbers of tetrahedral and octahedral substitutions are related to smectite components which vary between 37 and 81% with respect to the K atom numbers of I-S; this state was confirmed by total interlayer charge values of 0.33–0.75 eq/formula unit. Ca and Na from other interlayer cations have relatively small values (0.03–0.10 a.p.f.u.).

In the tetrahedral charge *vs.* octahedral charge ternary diagram (Figure 8a), R1 and R3 types of I-S fall within the theoretical I-S area between smectite and illite, indicating that tetrahedral charge changes from 0.6 to 0.75 eq/formula unit, but R0 type I-S or smectite-rich I-S is in the smectite area. The I-S compositions are between muscovite and celadonite and distributed from pyrophyllite to the middle point of the muscovite-celadonite line. They may also be distinguished from one another on the basis of ordering type, showing an arrangement typically from pyrophyllite to the illite point on the Si *vs.* Na+K compositional diagram (Figure 8b). R0 I-S (TAK-312) is close to the pyrophyllite corner, whereas R3 I-S is found near the illite point. In other words, ordering types of I-S were clearly separated from one another in both diagrams.

Table 3. Crystalchemical parameters of I-S and smectites from the Antalya unit.

Age	Formation	Unit	– KI (Δ°2θ) –		*b* cell dimension (Å)		—— Illite (%) in I-S ——		
			Interval	Mean	Interval	Mean	R3	R1	R0
Jura.-Cret.	Ballık	Rift-related formations	–	–	8.980–9.017	9.000	–	60–72	20–30
	Gökdere		–	–	8.990–9.005	8.998	–	70–75	40–50
	Çandır		0.31–0.79	0.48	8.991–9.017	9.009	88–93	70–85	30–55
Triassic	Karadere		0.70–0.78	0.74	8.994–9.017	9.007	87–95	70–80	30–56
	Tesbihli		–	–	–	–	–	70–80	40–55
	Kesmeköprü		0.36–0.95	0.46	9.010–9.020	9.015	86–93	70–80	–
	Dinek		0.60–0.75	0.68	8.991–9.020	9.009	88–91	65–80	–
Permian	Pamucakyayla	Pre-rift formations	0.50–0.63	0.57	–	–	89–95	73–84	–
Devonian	Hocanınsuyu		0.55–0.72	0.62	9.001–9.033	9.014	87–95	74–83	–
Silurian	Sapandere		0.32–0.77	0.51	9.007–9.027	9.015	89–95	80–84	–
Ordovician	Sarıyardere		0.30–0.52	0.43	–	–	89–94	70–84	–
	Seydişehir		0.27–0.60	0.42	9.006–9.014	9.010	89–94	70–84	–
Cambrian	Çaltepe		0.33–0.40	0.37	–	–	90–95	–	–

https://doi.org/10.1346/CCMN.2010.0580505 Published online by Cambridge University Press

Table 4. Major element composition (wt.%) and structural formulae for the fraction of I-S and smectite.

Unit	Tahtalıdağ nappe (pre-rift)	Alakırçay nappe (rift-related)							
Mineral	I-S					Smectite			
Ordering	R3	R3	R3>R1	R1>R0	R0>R1	– Dioctahedral		– Trioctahedral	
Oxide	TAK-103	TAK-39	TAK-179	TAK-24	TAK-312	TAK-227	TAK-227*	TAK-275	TAK-275*
SiO_2	52.93	52.46	53.53	51.45	54.34	59.40	59.55	43.79	45.14
TiO_2	1.181	0.434	0.780	0.646	0.517	0.196	0.197	2.071	2.130
Al_2O_3	22.17	24.06	18.96	20.63	22.01	20.47	20.66	12.34	12.72
ΣFe_2O_3	4.28	3.45	5.10	6.59	3.21	3.22	3.23	10.96	11.29
MnO	0.008	0.004	0.023	0.004	0.004	0.02	0.020	0.071	0.071
MgO	1.68	2.44	3.52	2.89	1.63	1.54	1.55	9.23	9.51
CaO	0.51	0.19	0.25	0.31	0.26	1.25	1.26	1.77	1.82
Na_2O	0.16	0.18	0.59	0.48	0.19	0.20	0.20	0.14	0.14
K_2O	6.84	7.25	5.50	4.71	2.08	0.43	0.01	2.95	0.01
P_2O_5	0.09	0.13	0.18	0.22	0.09	0.08	0.08	0.19	0.20
LOI	9.41	8.19	10.40	11.19	14.85	12.20	12.25	15.37	15.84
Total	99.26	98.80	98.83	99.12	99.18	99.01	99.01	98.87	98.87
Si	3.65	3.59	3.74	3.62	3.82		4.00		3.41
Al	0.35	0.41	0.26	0.38	0.18		0.00		0.59
TC	0.35	0.41	0.26	0.38	0.18		0.00		0.59
Ti	0.06	0.02	0.04	0.03	0.03		0.01		0.12
Al	1.46	1.52	1.30	1.33	1.65		1.64		0.55
Fe	0.22	0.18	0.27	0.35	0.17		0.16		0.64
Mg	0.17	0.25	0.37	0.29	0.16		0.16		0.96
TOC	1.91	1.97	1.98	2.00	2.00		1.97		2.27
OC	0.38	0.32	0.39	0.26	0.18		0.24		0.03
Mg	0.00	0.00	0.00	0.01	0.01		0.00		0.11
Ca	0.04	0.01	0.02	0.02	0.02		0.09		0.15
Na	0.02	0.02	0.08	0.07	0.03		0.03		0.02
K	0.60	0.63	0.49	0.42	0.19		0.00		0.00
P	0.01	0.01	0.01	0.01	0.01		0.01		0.01
ILC	0.75	0.72	0.66	0.64	0.33		0.26		0.59
TLC	0.73	0.73	0.65	0.60	0.36		0.24		0.62

* Calculated composition exluding theoretical muscovite composition, ΣFe_2O_3: Total iron, LOI: Loss on ignition, TC: Tetrahedral charge, TOC: Total octahedral cations, OC: Octahedral charge, ILC: Interlayer charge, TLC: Total layer charge.

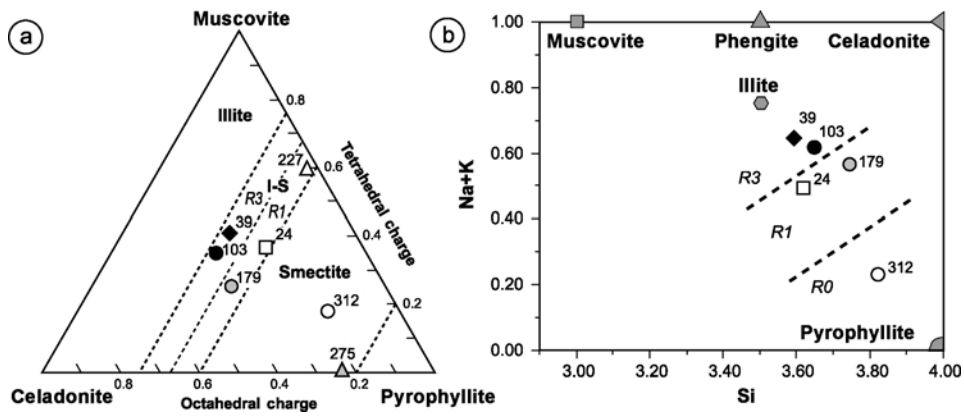

Figure 8. Plot of chemical data for smectite and I-S (dashed lines for R0, R1, and R3 were drawn on the basis of the data from this study). (a) Muscovite-celadonite-pyrophyllite ; (b) Na+K *vs.* Si.

https://doi.org/10.1346/CCMN.2010.0580505 Published online by Cambridge University Press

Dioctahedral and trioctahedral smectites plot in different areas of Figure 8a, as given below:

$(Ca_{0.09}Na_{0.03}P_{0.01})(Al_{1.64}Fe_{0.16}Mg_{0.16}Ti_{0.01})[Si_{4.00}Al_{0.00}O_{10}](OH)_2.2H_2O$

$(Mg_{0.11}Ca_{0.15}Na_{0.02}P_{0.01})(Al_{0.55}Fe_{0.64}Mg_{0.96}Ti_{0.12}[Si_{3.41}Al_{0.59}O_{10}](OH)_2.2H_2O$

In typical dioctahedral smectites, the charge ratio of tetrahedral to octahedral is <1.0 for montmorillonite, whereas it is >1.0 for beidellite (Güven, 1988). A dioctahedral smectite sample (TAK-227) has tetrahedral and octahedral charge values of 0.00 and 0.42 eq/formula unit, respectively, and is termed Mg-Fe-montmorillonite. Ca is the major interlayer cation (not Na). A trioctahedral smectite sample (TAK-275) contains some dioctahedral components and its tetrahedral and octahedral charge values are 0.59 and 0.03 eq/formula unit, respectively. The dominant charges for the tetrahedral and octahedral sites are characteristic of saponite and stevensite, respectively (Güven, 1988). Interlayer cations are Ca and Mg. The smaller value of total octahedral cations (2.27 a.p.f.u.) results from dioctahedral layers of ~30%, when compared to ideal trioctahedral smectite.

Trace-element and REE compositions

Trace-element concentrations, including *REE* values, of I-S and smectite (Table 5) reveal the trace-element contents of I-S in the pre-rift formations to be generally greater than those of the rift-related formations, except for Cu, Zn, Bi, and Sb. In other words, on the basis of their mean values, Cr and Co from the transition metals Sn, W, and Mo from granitoids: Rb, Ba, Sr, and Ga from the low-field-strength elements (LFSE); and Th and U from the high-field-strength elements (HFSE) are distinctly enriched, relatively speaking, in the pre-rift formations. This distinction indicates that elemental substitutions in I-S have occurred in the older formations. Similar to I-S, the trioctahedral smectite has a generally larger concentration than does the dioctahedral smectite, except for Pb, Sn, Cs, and Th. The smallest values of Sb, Ge, Ta, Nb, Hf, and Y were encountered in dioctahedral smectite, whereas the largest values of V, Cu, Zn, and Nb were detected in trioctahedral smectite.

When correlated with North American Shale Composite (NASC) values (Haskin *et al.*, 1968; Gromet *et al.*, 1984) of some trace elements and *REE*s, illite-rich I-S from pre-rift formations generally gives greater values than those of smectitic I-S from rift-related formations, and they are clearly distinguishable from one another (Figure 9b). In the R3 I-S of sample TAK-103 from the pre-rift Silurian Sapandere formation, all elements except for Rb, P, and Eu show greater values than those of the other I-S samples; in addition, Th and Sr give strong positive anomalies, whereas the anomaly for Eu is strongly negative. However, the R3 I-S of sample TAK-30 from the pre-rift Devonian Hocanınsuyu formation has lower concentrations, except for Rb, Th, K, Ta, La, Ce, Sr, and P, than those of both the R3 I-S of the Sapandere formation and the R1 and R0 I-S from the rift-related formations. In general, smectite-rich I-S has smaller values than those of illite-rich I-S, and their values are close to those of dioctahedral smectite. Both dioctahedral and trioctahedral smectites have the smallest values with respect to K, but dioctahedral smectite has the smallest elemental values, except for Ba, Th, Sr, and Eu, compared with trioctahedral smectite (Figure 9b). In addition, trioctahedral smectite suggests strong positive anomalies for P and Ti and negative for Ba and K.

The I-S of the pre-rift formations yields a broader range of total *REE* abundances, from 96.558 to 393.212 ppm, as well as high concentrations, compared to those of the rift-related formations. NASC-normalized total *REE* patterns of I-S and smectite are distinguishable from one another and indicate clear fractionation (Figure 10). The *REE* values show a v-shaped depletion relative to the NASC, except for R3 I-S from Sapandere formation, which has the greatest values of I-S (Figure 10a). In general, the light *REE* (*LREE*) concen-

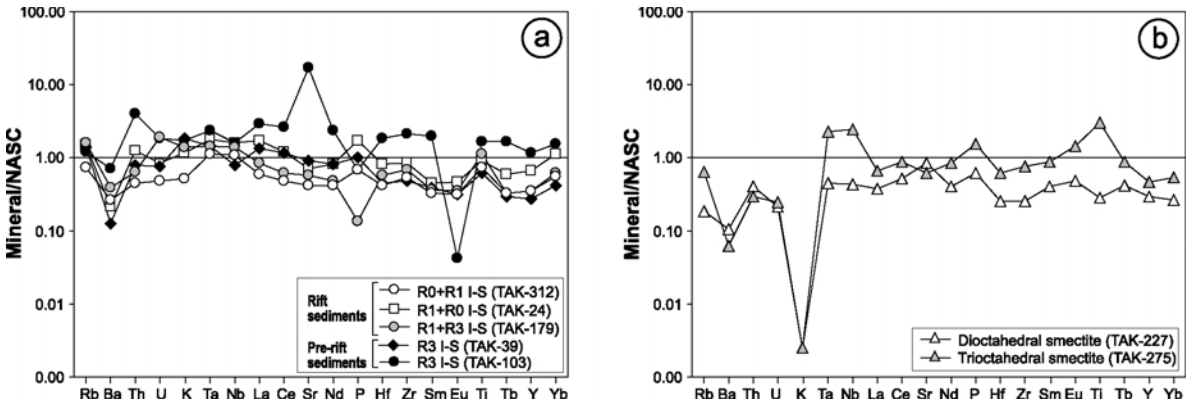

Figure 9. NASC-normalized trace-element patterns of (a) I-S and (b) smectite.

https://doi.org/10.1346/CCMN.2010.0580505 Published online by Cambridge University Press

Table 5. Trace element, *REE* (ppm) and isotopic compositions (‰) of I-S and smectite.

Unit	Tahtalıdağ nappe (pre-rift)		Alakırçay nappe (rift-related)				
Mineral	I-S					Smectite	
Ordering	R3	R3	R3>R1	R1>R0	R0>R1	Dioctahedral	Trioctahedral
Age	Silurian	Devonian	Triassic	Triassic	Triassic	Jura.-Cret.	Triassic
Sample no	TAK-103	TAK-39	TAK-179	TAK-24	TAK-312	TAK-227	TAK-275
Cr	130	230	340	170	100	90	160
Ni	50	50	30	50	30	70	170
Co	443	9	8	7	4	29	53
Sc	14	8	14	14	10	13	30
V	114	86	182	149	92	118	271
Cu	<10	<10	10	50	60	60	80
Pb	12	<5	7	<5	<5	9	<5
Zn	120	70	10	110	70	120	130
Bi	0.3	<0.1	<0.1	0.5	0.3	0.3	<0.1
In	<0.1	<0.1	<0.1	<0.1	<0.1	<0.1	<0.1
Sn	5	3	4	4	2	2	1
W	354.0	56.7	25.8	4.2	10.7	6.6	10.6
Mo	3	10	24	6	4	<2	<2
As	<5	<5	13	<5	<5	6	<5
Sb	2.0	0.6	2.3	2.1	1.8	<0.2	2.7
Ge	1.2	1.2	2.3	1.8	1.5	0.7	1.6
Be	2	2	3	2	1	1	1
Ag	<0.5	<0.5	<0.5	<0.5	<0.5	<0.5	<0.5
Rb	149	174	198	187	92	23	80
Cs	4.4	9.7	13.6	11.9	7.0	1.6	0.8
Ba	459	81	246	136	171	67	39
Sr	2421	129	81	101	60	122	88
Tl	0.61	0.67	0.77	00.67	0.44	0.29	0.07
Ga	30	25	26	29	14	19	16
Ta	2.65	1.62	1.61	2.03	1.25	0.51	2.57
Nb	20.9	10.4	18.0	21.2	14.1	5.7	31.9
Hf	11.5	2.8	3.6	5.2	2.6	1.6	3.9
Zr	422	96	137	173	108	51	155
Y	40.4	9.7	12.5	23.4	12.5	10.2	16.1
Th	49.70	9.79	7.95	15.20	5.49	4.95	3.64
U	4.94	2.04	5.08	2.30	1.28	0.58	0.66
La	90.20	41.30	26.80	53.10	18.80	11.80	20.30
Ce	177.0	78.7	41.8	81.9	32.0	34.5	58.4
Pr	18.00	7.31	4.03	7.96	3.30	2.80	5.85
Nd	64.20	22.50	13.30	22.80	11.50	11.10	23.50
Sm	11.10	2.20	2.04	2.49	1.82	2.30	4.97
Eu	0.050	0.379	0.410	0.545	0.378	0.562	1.710
Gd	8.46	1.32	1.38	2.03	1.35	2.12	4.53
Tb	1.40	0.25	0.28	0.50	0.28	0.36	0.74
Dy	8.08	1.66	2.04	3.80	2.04	1.91	4.11
Ho	1.63	0.38	0.47	0.88	0.46	0.34	0.73
Er	4.96	1.25	1.58	3.07	1.52	0.92	2.00
Tm	0.734	0.201	0.272	0.511	0.256	0.131	0.273
Yb	4.67	1.30	1.87	3.47	1.69	0.80	1.65
Lu	0.728	0.199	0.286	0.488	0.256	0.110	0.233
$\delta^{18}O$ (SMOW)	17.4	17.7	21.2	23.2	26.3	27.9	25.9
δD (SMOW)	−69	−76	−75	−100	−95	−90	−103
Σ*REE*	393.212	158.949	96.558	183.544	75.650	69.753	128.996
La_N/Lu_N	13.279	22.242	10.043	11.662	7.871	11.497	9.337
Eu/Eu*	0.647	0.680	0.747	0.741	0.732	0.778	1.102

Σ*REE* = total *REE*, Eu/Eu*= $Eu_N/(Sm_N.Gd_N)^{0.5}$

https://doi.org/10.1346/CCMN.2010.0580505 Published online by Cambridge University Press

trations are slightly depleted with respect to heavy *REE* (*HREE*) concentrations. The amounts of *REE* in I-S increase in pre-rift formations relative to rift-related formations, while two samples of R3 I-S from the pre-rift formations are fairly different (Figure 10a). The pattern of the NASC-normalized average *REE* values for pre-rift and rift-related I-S (Figure 10b) indicates that the R3 I-S from the pre-rift formations is clearly enriched in *LREE* relative to R0 and R1 from the rift-related formations, whereas there is little enrichment of *HREE*. In addition, the *REE* value of trioctahedral smectite is greater than that of dioctahedral smectite, and has a trend similar to *REE* values of dioctahedral smectite (Figure 10c).

Chondrite-normalized Eu/Eu* (Sun and McDonough, 1989; Taylor and McLennan, 1985), NASC-normalized La_N/Lu_N ratios, and the K_2O contents of I-S are noteworthy relationships between *REE* and increasing K_2O, reflecting increasing diagenetic/metamorphic grade (Figure 11a,b). In addition, La_N/Lu_N ratios of I-S, in opposition to Eu/Eu* ratios, increase together with K_2O contents.

Oxygen and hydrogen isotopes

Stable-isotope compositions of two smectite and five I-S samples (Table 5) showed that the $\delta^{18}O$ values vary from +17.4 to 27.9 (SMOW)‰, whereas those of δD are scattered over a relatively wide interval, −69 to −103 (SMOW)‰. The $\delta^{18}O$ and δD ranges of the clay minerals are given in Figure 12, together with the

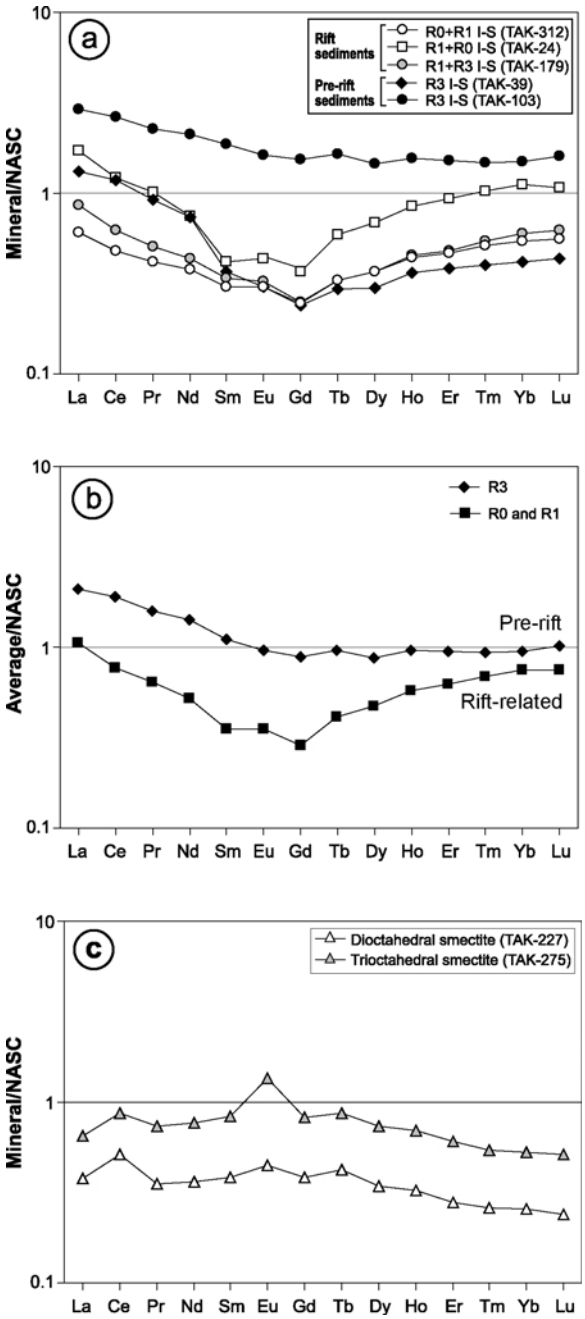

Figure 10. NASC-normalized *REE* patterns (Ho and Tm values from Haskin *et al.*, 1968, and the other elements from Gromet *et al.*, 1984 for NASC). (a,b) I-S; (c) smectites.

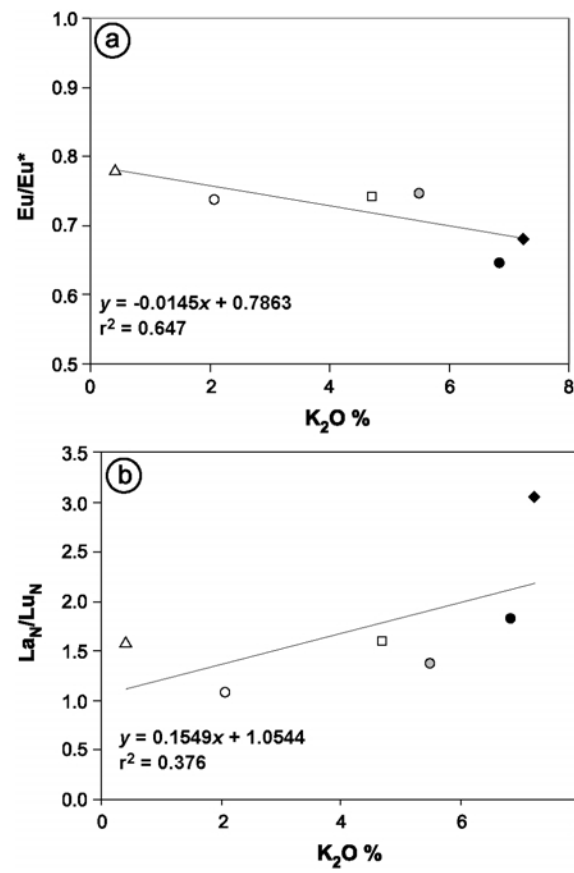

Figure 11. (a) Chondrite-nomalized Eu/Eu* and (b) NASC-normalized La_N/Lu_N ratios of smectite and I-S *vs.* K_2O wt.%. (symbols as in Fig. 9).

https://doi.org/10.1346/CCMN.2010.0580505 Published online by Cambridge University Press

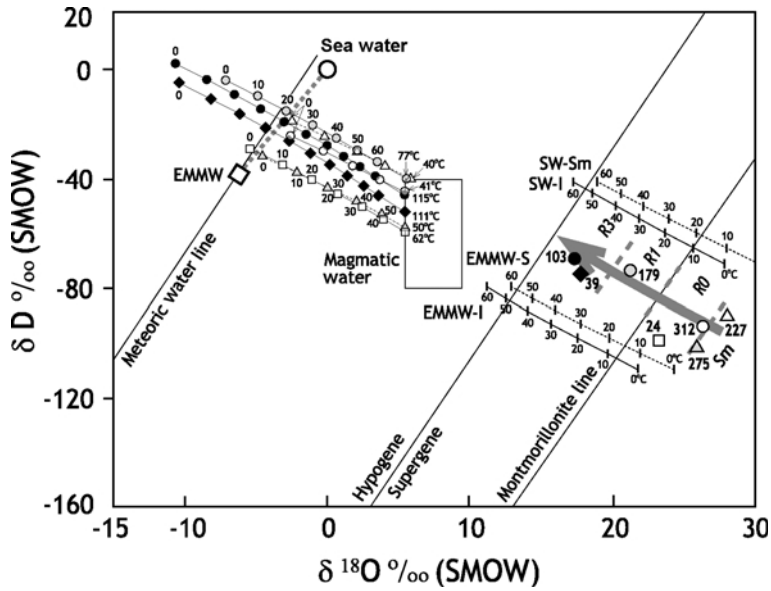

Figure 12. Plot of δD *vs*. $\delta^{18}O$ values of mineral and mineral-water equilibria for smectite and I-S minerals. Compositions of smectite and illite in equilibrium with sea water and EMMW for temperature (ºC) were also given for comparison. The arrow indicates an isotopic fractionation trend from smectite to R3 I-S. Dashed lines for R0, R1, and R3 were drawn on the basis of the data from the present study.

meteoric water line (Craig, 1961), the lines for supergene-hypogene origin (Sheppard *et al.*, 1969), and for montmorillonite (Savin and Epstein, 1970). Isotopic-fractionation trends, with respect to temperature from smectite-water and illite-water in equilibrium with Sea Water (SW) and Eastern Mediterranean Meteoric Water (EMMW, $\delta^{18}O = -6.12‰$, $\delta D = -37.96‰$, Gat *et al.*, 1996), and also magmatic water ($\delta^{18}O = 5.5$ to 9.5 ‰, $\delta D = -40$ to $-80‰$, Sheppard *et al.*, 1969), have also been drawn, and the following equations were used for the smectite-water and illite-water fractionation factors:

Oxygen: $1000 \ln\alpha_{(\text{smectite-water})} = 2.58 \times 10^6 T^{-2} - 4.19$
Savin and Lee (1988)

$1000 \ln\alpha_{(\text{illite-water})} = 2.39 \times 10^6 T^{-2} - 4.19$
Savin and Lee (1988)

Hydrogen: $1000 \ln\alpha_{(\text{illite/smectite-water})} =$
$-45.3 \times 10^3/T + 94.7$
Capuano (1992)

Clay samples of the Antalya Unit reflect wholly supergene conditions. Smectites are situated in the right part of the diagram, corresponding to the lowest-temperature conditions, whereas I-S samples have a linear arrangement (according to their ordering types) toward decreasing $\delta^{18}O$ and increasing δD. Isotopic data for the smectites and I-S plot between SW and EMMW, indicating that the waters involved in the formation of clay minerals in the Antalya Unit are of mixed character. In addition to $\delta^{18}O$ values of I-S, which reveal a regular distribution with increasing diagenetic grade and K_2O (Figure 13), δD values are lowest, suggesting a different isotopic evolution for clays of the rift-related extensional basin. Even if the oxygen isotopes are more reliable than hydrogen isotopes at indicating temperature relations in the clay minerals (Longstaffe and Ayalon, 1990), hydrogen-isotope fractionation is as significant as oxygen fractionation in the studied samples.

DISCUSSION

The sequence studied played an important role in the Paleozoic and Mesozoic evolution of the southern Tauride Belt in the context of the NW margin of Gondwana. Prior to Late Permian time, the easternmost Mediterranean area formed part of the northern margin of Gondwana, and remnants of the extensional setting – evidence of Late Triassic rifting – are preserved in the Antalya Unit (Robertson, 2000). In the Alanya-Gazipaşa area, the eastern extension of the Antalya Unit, pre-Permian parts of the Antalya Unit are represented by only one formation, comprising siliciclastic and scarce carbonate rocks of Cambrian–Ordovician age (Ulu, 1983; Özgül, 1984; Göncüoğlu and Kozur, 1999; Bozkaya and Yalçın, 2005). Triassic volcanic rocks and radiolarite-bearing siliceous rocks are relatively scarce in this area. In addition, some diagenetic and mineralogical characteristics of the pre-rift and rift-related units are different from those of the Kemer-Kumluca area, *vis-à-vis* the greater diagenetic/metamorphic grade, *i.e.* higher grade as reflected by KI

https://doi.org/10.1346/CCMN.2010.0580505 Published online by Cambridge University Press

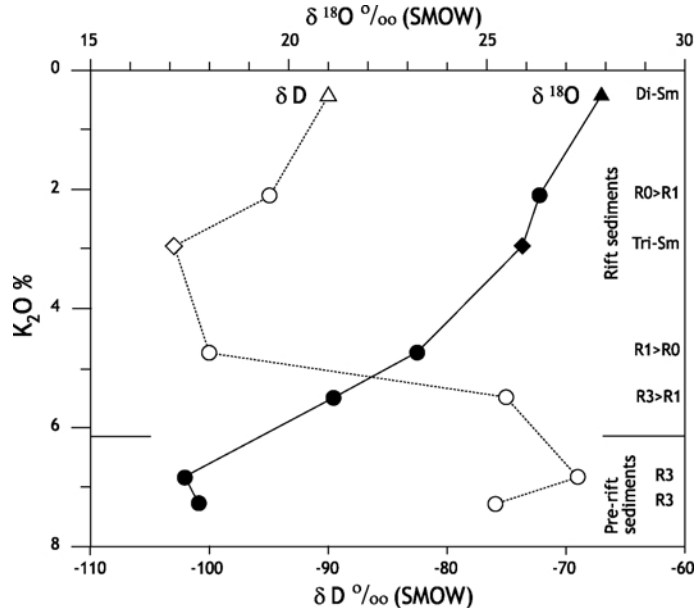

Figure 13. Distribution of δD and $\delta^{18}O$ values of smectite and I-S minerals together with K_2O wt.% and ordering type of I-S.

values, dominance of $2M_1$ illite, and the absence of I-S (Bozkaya and Yalçın, 2005). These differences seem to be related to different thermal and tectonic histories for tectonostratigraphic units of the regions.

On the basis of the vertical distribution of mineralogical data (Figure 14a), the types and abundances of minerals appear to be mainly related to provenance and depositional environment. The presence of feldspar together with chlorite and C-S in the clastic-rich levels of the Silurian Sarıyardere formation indicates a volcanic source. The disappearance of kaolinite and C-S throughout the pre-rift Sarıyardere and Sapandere formations seems to have been related to different thermal histories and/or stratigraphic discontinuities prior to rifting. The drastic drop in KI and *b* values from the Silurian to the Ordovician may also be interpreted as different thermal evolutions for the two formations. Similar mineralogical differences are found, in part, between the Sapandere and Hocanınsuyu formations with their discordant boundary. Chemical depletions, namely, trace-element and *REE* values (see Figures 9, 10), corroborate these different histories. In this context, the presence of a regional unconformity on the Ordovician, and an angular unconformity between the Devonian and older units, are evidence of characteristic events in several units of the Tauride Belt, as previously emphasized by Göncüoğlu and Kozlu (2000). The contrasting relationships between calcite and quartz contents in the rift-related sediments are related to chemical-precipitation settings, such as in the shallow and deeper parts of the basin, respectively. Calcite in the Gökdere formation developed in the shallow parts; whereas quartz in the Ballık formation reflects development in deeper parts (below the carbonate compensation depth) of the basin (see Figure 2). Feldspar is scarce or absent in the rift-related formations, except for the Karadere and Çandır formations which are made up of volcanogenic materials. In addition to increasing amounts of feldspar and chlorite, the appearance of C-S, analcime, tetranatrolite, and hydroxyapophyllite clearly support a volcanic origin. Polytype characterization of R3 I-S-rich fractions, and $1M_d$ or $1M + 1M_d$, indicate that they are diagenetic in origin and do not contain any detrital illite/mica with the $2M_1$ polytype, which has high-grade diagenetic to low metamorphic grade (*e.g.* Frey, 1987; Grathoff and Moore, 2002). Such an evaluation, based on the petrographic observations, is confirmed by the absence of detrital mica fragments in the I-S-bearing samples.

The lithologic and mineralogic-petrographic characteristics of the analyzed samples (see Table 1) suggest that the smectite and I-S originated from volcanogenic and clastic/calcareous rocks, respectively. Ordering types and/or illite percentages in I-S reflect different diagenetic grades related to increasing depth rather than to lithologic and mineralogic differences (*e.g.* Abid *et al*., 2004). Similarly, regular increase in K_2O and Al_2O_3, together with decrease in SiO_2 and CaO, can be linked to increasing diagenetic grade (Figure 14b). If the interlayer K of illite is assumed to be 0.7, K atom numbers of I-S (0.19–0.63 a.p.f.u., see Table 3) indicate 27–90% illite or 10–73% smectite layers. The values were confirmed by XRD studies, as were the presence of the R0 (10–55 I%), R1 (55–85 I%), and R3 (85–95 I%) types of I-S.

Variations in trace-element and, in particular, *REE* distributions in the I-S with different ordering types

https://doi.org/10.1346/CCMN.2010.0580505 Published online by Cambridge University Press

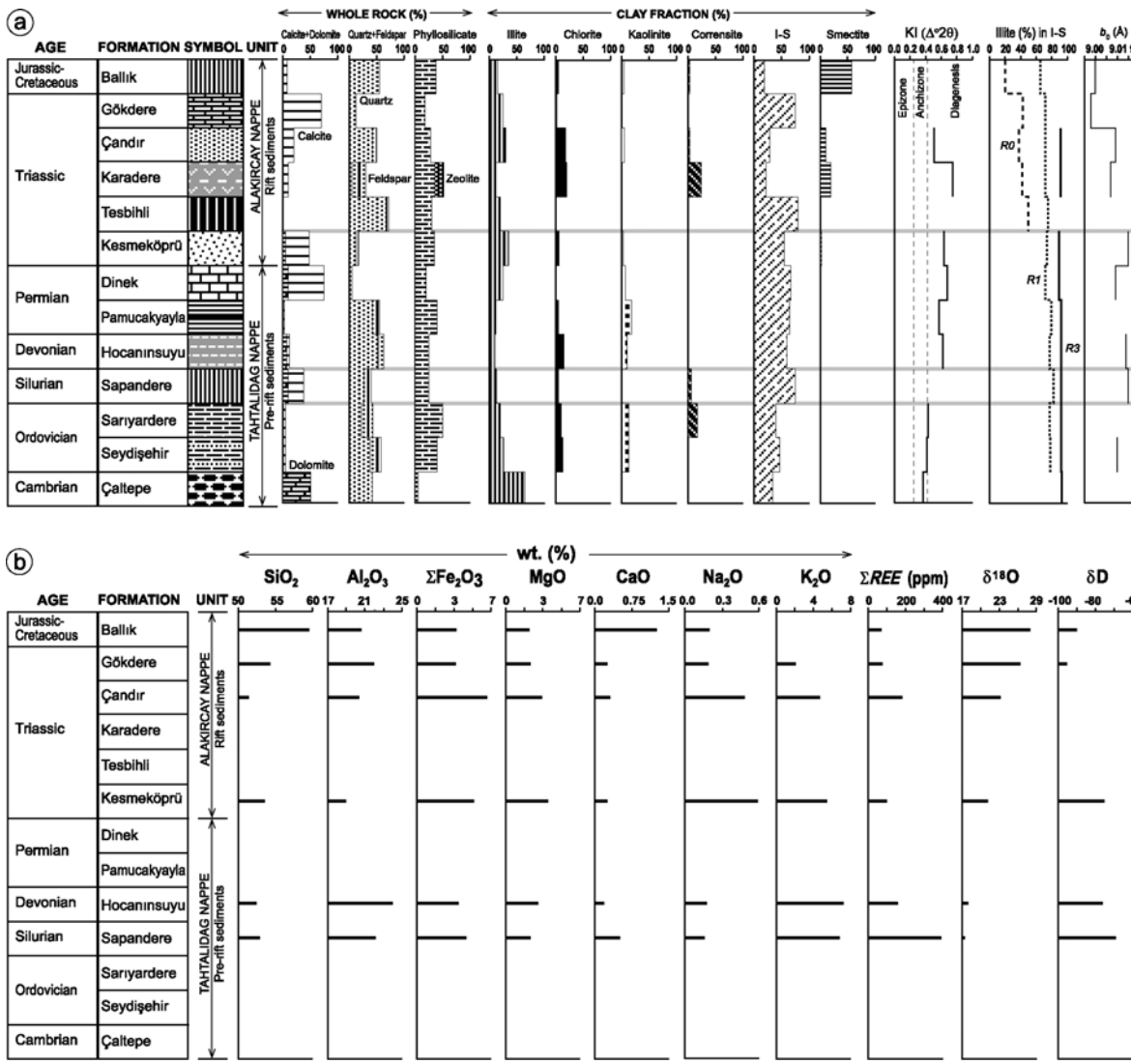

Figure 14. Vertical distributions of (a) mineralogical and (b) geochemical data of pre-rift and rift-related formations from the Antalya Unit.

reflects change in diagenetic grade or increasing temperature, as established by some researchers (*e.g.* Awwiller and Mack, 1991; Milodowski and Zalaciewicz, 1991; Ohr *et al.*, 1994). However, remarkable extreme values in R3 I-S samples from the Silurian Sapandere formation should arise from accessory heavy minerals (*e.g.* Honty *et al.*, 2008), a conclusion supported by the presence of anatase and hematite granules (0.3–0.7 μm size) on I-S flakes, as noted during earlier SEM investigations of this sample (Bozkaya and Yalçın, 2007). The *HREE* contents of trioctahedral smectite rather than those of dioctahedral smectite, I-S, and NASC may be evaluated insofar as they were derived from lava. The *REE* contents of the smectite-type fractions are relatively immobile in glass-clay reactions, and, therefore, are quite large (*e.g.* Zielinski, 1982); the main loss might result from the fact that the *REE*s are associated with the genesis of Mg-smectite. Conversely, the smaller values of the dioctahedral smectites are considered to have been derived from altered glass, found to be lower than those of the NASC (*e.g.* Elliott, 1993). The Eu anomaly (Eu/Eu*) shows a nearly regular decrease with increasing K_2O or illite contents in I-S, together with increasing diagenetic grades or K_2O contents of the Antalya Unit (Figure 11a). The Eu anomaly generally reflects a specific origin, mobility, or fractionation (*e.g.* Uysal and Golding, 2003; Honty *et al.*, 2008). Increasing Eu anomalies – from pre-rift to rift-related I-S and maximum values for smectites – may be explained by volcanogenic feldspar, considered to be a reference-mineral phase controlling Eu mobility. The largest Eu anomaly in the trioctahedral smectite was

https://doi.org/10.1346/CCMN.2010.0580505 Published online by Cambridge University Press

apparently derived by alteration of basaltic lava due to varying amounts of feldspar. La_N/Lu_N ratios of I-S and smectite, reflecting *HREE* enrichment relative to *LREE*, have an almost regular distribution – increasing from smectite to R3 I-S in relation to their K_2O contents (see Figure 11b) – thus indicating the positive relation between La_N or L*REE* and illite interlayers. The *LREE* can only fit in the illite interlayers, and thus the I-S interlayer sites should preferentially accumulate *LREE*s relative to *HREE*s during progressive illitization if I-S mineralization controls *REE* fractionation (Awwiller, 1994).

Isotope fractionation of smectites and I-S calculated from the equations of Savin and Lee (1988) yields fairly low-temperature data – ~0ºC for smectites and R0 I-S, ~20ºC for R1 I-S, and ~40ºC for R3 I-S (see Figure 12) – when the primary water composition is assumed to be sea water and EMMW. These temperatures are anomalously lower than expected for an extensional basin. On the basis of mineralogical data, the R3 I-S has late-diagenetic KI indices, and thus the temperature conditions of the clays must have been greater than the measured values. For the higher-temperature values, magmatic water is envisioned to have been introduced to the formation water. If the primary water composition was completely magmatic in origin, the calculated minimum temperature values would be 40–115ºC. The isotopic composition of the formation waters of the clay minerals suggests that the available water (a mixture of sea water and meteoric water) mixed with magmatic water. In other words, magmatic water input is dominant for smectite occurrences, whereas meteoric and sea water contributions are relatively high for I-S synthesis. The approach seems to be supported by the presence of volcanic activity during the extension of the basin. Isotopic-temperature variations among Devonian and Triassic units reached up to 50ºC; the difference in temperature from the burial diagenetic areas with a normal geothermal gradient (25–30ºC/km) suggests a burial depth of ~2000 m, which disagrees with actual findings insofar as the Triassic sequences of the Antalya Unit have a maximum depth of 1000 m. The wide range in hydrogen- and oxygen-isotopic values indicate that hydrogen-isotope values were not changed and rearranged during post-diagenetic processes, as mentioned by Longstaffe and Ayalon (1990). The observation of regular isotopic distribution together with increasing temperature indicate progressive changes in the formation waters of clay minerals of the Antalya Unit along with increasing time and depth, as suggested for fluid-rock interactions by Bechtel *et al.* (1999).

CONCLUSIONS

The KI of illites, illite content (%), and interstratification of I-S reflect increasing diagenetic/metamorphic character with depth – from early diagenetic to low anchimetamorphic grades. Cambrian-Ordovician units have anchimetamorphic–late-diagenetic characteristics, whereas Silurian–Permian sections reflect entirely late-diagenetic conditions in pre-rift units of the Tahtalıdağ nappe, indicating the presence of an earlier thermal event prior to Triassic rifting. The Triassic parts of the rift-related Alakırçay nappe are characterized by late- to early-diagenetic features, but the Jurassic–Cretaceous parts have early-diagenetic grades, related to basin maturity during rifting.

The different types of I-S interstratification (as R0, R1, and R3), the illite contents of the I-S (29–87%), and the interlayer K+Na contents increase from R0 to R3 I-S. Mg-Fe montmorillonite and Al-Fe saponite from the smectites represent clay-sized traces from *in situ* alteration of Triassic lavas and Jurassic pyroclastic products.

The total trace-element concentrations of the I-S are greater than those of the smectites. Except for extreme values, on the basis of mean clay contents, transition metals are enriched in smectite, whereas most of the 'granitoid elements' (LFSE and HFSE) are dominant in the structure of the I-S. Trace-element concentrations of I-S from pre-rift sediments are larger than those of rift-related sediments; similar situations are observed in trioctahedral and dioctahedral smectites. In NASC-normalized *REE* patterns, elemental fractionation is greatest for the smectites but least for the I-S, thus suggesting magmatic and sedimentary provenance, respectively.

On the basis of the oxygen- and hydrogen-isotopic compositions of these clays, the smectites and I-S suggest entirely supergene conditions and a progressive isotopic fractionation trend from smectite to R3 I-S with increasing temperature, along with decreasing $\delta^{18}O$ and increasing δD values. This evolution is also confirmed by the increasing K_2O contents of I-S. The formation water of the clays was a mixture of sea-water, EMMW, and magmatic-water compositions. The δD values are characteristic of extension or rifting as opposed to the $\delta^{18}O$ values, and greater δD values for the I-S are of rift sediments, whereas pre-rift sediments have smaller values. According to isotopic-temperature differences among the Devonian and Triassic units, diagenesis of the Antalya Unit was probably at a greater geothermal gradient (>35ºC/km), demonstrating that typical extensional-basin conditions were caused by high heat flow. Finally, major-element, trace-element, *REE*, and stable-isotope values of the I-S and smectites indicate that geochemical signals were controlled by diagenetic grade, and that these can be used to monitor basin maturity along with mineralogical data.

ACKNOWLEDGMENTS

The present study was supported by The Scientific and Technological Research Council of Turkey (TÜBİTAK) within the framework of Project No. 104Y329. The XRD measurements and thin-section preparation were carried

out by F. Yalçin and U. Kus. The authors gratefully acknowledge D. Hozatlioglu and Z. Basibuyuk for their assistance in the laboratory. W.D. Huff and S.K. Mittwede kindly read the manuscript and are thanked for their constructive comments. The authors are particularly grateful to L.B. Williams, H. Dypvik, and an anonymous referee for their comprehensive reviews and valuable comments.

REFERENCES

Abid, I.A., Hesse, R., and Harper, J.D. (2004) Variations in mixed-layer illite/smectite diagenesis in the rift and post-rift sediments of the Jeanne d'Arc Basin, Grand Banks offshore Newfoundland, Canada. *Canadian Journal of Earth Sciences*, **41**, 401–429.

Awwiller, D.N. (1994) Geochronology and mass transfer in Gulf Coast mudrocks (south-central Texas, U.S.A.): Rb-Sr, Sm-Nd and REE systematics. *Chemical Geology*, **116**, 61–84.

Awwiller, D.N. and Mack, L.F. (1991) Diagenetic modifications of Sm-Nd model ages in Tertiary sandstones and shales, Texas Gulf Coast. *Geology*, **19**, 311–314.

Bechtel, A., Savin, S.M., and Hoernes, S. (1999) Oxygen and hydrogen isotopic of clay minerals of the Bahloul Formation in the region of the Bou Grine zinc-lead ore deposit (Tunisia): evidence for fluid-rock interaction in the vicinity of salt dome cap rock. *Chemical Geology*, **156**, 191–207.

Bozkaya, Ö. and Yalçın, H. (2004a) Diagenetic to low-grade metamorphic evolution of clay mineral assemblages in Palaeozoic to early Mesozoic rocks of the Eastern Taurides, Turkey. *Clay Minerals*, **39**, 481–500.

Bozkaya, Ö. and Yalçın, H. (2004b) New mineralogical data and implications for the tectono-metamorphic evolution of the Alanya Nappes, Central Tauride Belt, Turkey. *International Geology Review*, **46**, 347–365.

Bozkaya, Ö. and Yalçın, H. (2005) Diagenesis and very low-grade metamorphism of the Antalya Unit: mineralogical evidence of Triassic rifting, Alanya-Gazipaşa, Central Taurus Belt, Turkey. *Journal of Asian Earth Sciences*, **25**, 109–119.

Bozkaya, Ö. and Yalçın, H. (2007) *Investigation of diagenetic/metamorphic grade of the Antalya Unit (Tahtalıdağ and Alakırçay nappes)*. The Scientific and Technological Research Council of Turkey (TUBITAK), Project No: 104Y329, 130 pp.

Bozkaya, Ö., Yalçın, H., and Göncüoğlu, M.C. (2002) Mineralogic and organic responses to the stratigraphic irregularities: an example from the Lower Paleozoic very low-grade metamorphic units of the Eastern Taurus Autochthon, Turkey. *Schweizerische Mineralogische und Petrographische Mitteilungen*, **82**, 355–373.

Bozkaya, Ö., Gürsu, S., and Göncüoğlu, M.C. (2006) Textural and mineralogical evidence for a Cadomian tectonothermal event in the eastern Mediterranean (Sandıklı-Afyon area, western Taurides, Turkey). *Gondwana Research*, **10**, 301–315.

Brindley, G.W. (1980) Quantitative X-ray mineral analysis of clays. Pp. 411–438 in: *Crystal Structures of Clay Minerals and their X-ray Identification* (G.W. Brindley and G. Brown, editors). Monograph **5**, Mineralogical Society, London.

Brunn, J.H., Dumont, J.F., De Graciansky, P.C., Gutnic, M., Juteau, T., Marcoux, J., Monod, O., and Poisson, A. (1971) Outline of the geology of the western Taurides. Pp. 225–255 in: *Geology and History of Turkey* (A.S. Campbell, editor). Petroleum Exploration Society of Libya, Tripoli.

Capuano, R.M. (1992) The temperature dependence of H-isotope fractionation between clay minerals and water: Evidence from a geopressured system. *Geochimica et Cosmochimica Acta*, **56**, 2547–2554.

Clayton, R.N. and Mayeda, T.K. (1963) The use of bromine pentafluoride in the extraction of oxygen from oxides and silicates for isotopic analysis. *Geochimica et Cosmochimica Acta*, **27**, 43–52.

Condie, K.C. (1991) Another look at rare earth elements in shales. *Geochimica et Cosmochimica Acta*, **55**, 2527–2537.

Craig, H. (1961) Isotopic variations in meteoric waters. *Science*, **133**, 1702–1703.

Dumont, J.F., Gutnic, M., Marcoux, J., Monod, O., and Poisson, A. (1972) Le Trias des Taurides occidantales (Turquie). Définition du bassin pamphylien: Un nouveau domaine à la marge éxterne de la chaine taurique. *Zeitschrift der Deutsche Geologischen Gesellschaft*, **123**, 385–409.

Elliott, W.C. (1993) Origin of the Mg-smectite at the Cretaceous/Tertiary (K/T) boundary at Stevns Klint, Denmark. *Clays and Clay Minerals*, **41**, 442–452.

Fleet, A.J. (1984) Aqueous and sedimentary geochemistry of the rare earth elements. Pp. 343–373 in: *Rare Earth Elements* (P. Henderson, editor). Developments in Geochemistry, **2**, Elsevier, Amsterdam.

Frey, M. (1987) Very low-grade metamorphism of clastic sedimentary rocks. Pp. 9–58 in: *Low-Temperature Metamorphism* (M. Frey, editor). Blackie and Son, Glasgow, UK.

Folk, R.L. (1968) *Petrology of Sedimentary Rocks*. University of Texas Publications, Austin, Texas, USA, 170 pp.

Gat, J.R., Shemesh, A., Tziperman, E., Hecht, A., Georgopoulus, D., and Basturk, O. (1996) The stable isotope composition of waters of the eastern Mediterranean Sea. *Journal of Geophysical Research*, **101**, 6441–6451.

Göncüoğlu, M.C. and Kozlu, H. (2000) Early Paleozoic evolution of the NW Gondwanaland: data from southern Turkey and surrounding regions. *Gondwana Research*, **3**, 315–324.

Göncüoğlu, Y. and Kozur, H.W. (1999) Upper Cambrian and Lower Ordovician conodonts from the Antalya unit in the Alanya Tectonic Window, southern Turkey. *Neues Jahrbuch für Geologie Palaontologie Monatshefte*, **10**, 593–604.

Göncüoğlu, M.C., Dirik, K., and Kozlu, H. (1997) General characteristics of pre-Alpine and Alpine Terranes in Turkey: Explanatory notes to the terrane map of Turkey. Annales Geologique de Pays Hellenique, **37**, *Geological Society of Greece*, 515–536.

Grathoff, G.H. and Moore, D.M. (2002) Characterization of the Waukesha Illite: a mixed-polytype illite in the Clay Minerals Society repository. *American Mineralogist*, **87**, 1557–1563.

Gromet, L.P., Dymek, R.F., Haskin, L.A., and Korotev, R.L. (1984) The North American shale composite: Its compilation, major and trace element characteristics. *Geochimica et Cosmochimica Acta*, **48**, 2469–2482.

Guggenheim, S., Bain, D.C., Bergaya, F., Brigatti, M.F., Drits, V.A., Eberl, D.D., Formoso M.L.L., Galán, E., Merriman, R.J., Peacor, D.R., Stanjek, H., and Watanabe T. (2002) Report of the AIPEA nomenclature committee for 2001: order, disorder and crystallinity in phyllosilicates and the use of the "Crystallinity Index". *Clay Minerals*, **37**, 389–393.

Güven, N. (1988) Smectites. Pp. 497–560 in: *Hydrous Phyllosilicates*, (S.W. Bailey, editor). Reviews in Mineralogy, **19**, Mineralogical Society of America, Washington D.C.

Haskin, L.A., Haskin, M.A., Frey, F.A., and Wideman, T.R. (1968) Relative and absolute terrestrial abundances of the rare earths. Pp. 880–912 in: *Origin and Distribution of the Elements* (L.H. Ahrens, editor). Pergamon Press, Oxford, UK.

Honty, M., Clauer, N., and Šucha, V. (2008) Rare-earth elemental systematics of mixed-layered illite-smectite from sedimentary and hydrothermal environments of the Western Carpathians (Slovakia). *Chemical Geology*, **249**, 167–190.

Hower, J., Eslinger, E.V., Hower, M.E., and Perry, E.A. (1976) Mechanism of burial metamorphism of argillaceous sediment: 1. Mineralogical and chemical evidence. *Geological Society of America Bulletin*, 87, 725–737.

Kalafatçıoğlu, A. (1973) Antalya körfezi batı kesiminin jeolojisi. *Bulletin of the Mineral Research and Exploration of Turkey*, **81**, 82–131 (in Turkish).

Kisch, H.J. (1980) Illite crystallinity and coal rank associated with lowest-grade metamorphism of the Taveyanne greywacke in the Helvetic zone of the Swiss Alps. *Eclogae Geologicae Helvetiae*, **73**, 753–777.

Kisch, H.J. (1991a) Illite crystallinity: recommendations on sample preparation, X-ray diffraction settings, and interlaboratory samples. *Journal of Metamorphic Geology*, **9**, 665–670.

Kisch, H.J. (1991b) Development of slaty cleavage and degree of very-low-grade metamorphism: a review. *Journal of Metamorphic Geology*, **9**, 735–750.

Krumm, S. (1996) *WINFIT 1.2*: version of November 1996 (The Erlangen geological and mineralogical software collection) of "WINFIT 1.0: a public domain program for interactive profile-analysis under WINDOWS". XIII Conference on Clay Mineralogy and Petrology, Praha, 1994. *Acta Universitatis Carolinae Geologica*, **38**, 253–261.

Kübler, B. (1968) Evaluation quantitative du métamorphisme par la cristallinité de l'illite. *Bulletin-Centre de Recherches Pau-SNPA*, **2**, 385–397.

Longstaffe, F.J. and Ayalon, A. (1990) Hydrogen-isotope geochemistry of diagenetic clay minerals from Cretaceous sandstones, Alberta: evidence for exchange. *Applied Geochemistry*, **5**, 657–688.

Maury, R.C., Lapierre, H., Bosch, D., Marcoux, J., Krystyn, L., Cotton, J., Bussy, F., Brunet, P., and Senebier, F. (2008) The alkaline intraplate volcanism of the Antalya nappes (Turkey): a Late Triassic remnant of the Neotethys. *Bulletin de la Société Geologique de France*, **179**, 397–410.

McLennan, S.M. (1989) Rare earth elements in sedimentary rocks: influence of provenance and sedimentary processes. Pp. 169–200 in: *Geochemistry and Mineralogy of Rare Earth Elements* (B.R. Lipin and G.A. McKay, editors). Reviews in Mineralogy, **21**. Mineralogical Society of America, Washington, D.C.

Merriman R.J. (2005) Clay minerals and sedimentary basin history. *European Journal of Mineralogy*, **17**, 7–20.

Merriman, R.J. and Frey, M. (1999) Patterns of very low-grade metamorphism in metapelitic rocks. Pp. 61–107 in: *Low Grade Metamorphism* (D. Robinson and M. Frey, editors). Blackwell Science, Oxford, UK.

Merriman, R.J. and Peacor, D.R. (1999) Very low grade metapelites: Mineralogy, microfabrics and measuring reaction progress. Pp. 10–60 in: *Low-Grade Metamorphism* (D. Robinson and M. Frey, editors), Blackwell Science, Oxford, UK.

Milodowski, A.E. and Zalasiewicz, J.A. (1991) Redistribution of rare earth elements during diagenesis of turbidite/hemipelagite mudrock sequences of Llandovery age from Central Wales. Pp. 101–124 in: *Developments in Sedimentary Provenance Studies* (A.C. Morton, S.P. Todd and P.D.W. Haughton, editors). Special Publications, **57**, Geological Society of London.

Moore, D.M. and Reynolds, R.C. (1997) *X-ray Diffraction and the Identification and Analysis of Clay Minerals*. Oxford University Press, New York.

O'Brien, N.R. and Slatt, R.M. (1990) *Argillaceous Rock Atlas*. Springer-Verlag, New York.

Ohr, M., Halliday, A.N., and Peacor, D.R. (1994) Mobility and fractionation of rare earth elements in argillaceous sediments: implications for dating diagenesis and low-grade metamorphism. *Geochimica et Cosmochimica Acta*, **58**, 289–312.

Özgül, N. (1976) Some geological aspects of the Taurus orogenic belt (Turkey). *Bulletin of the Geological Society of Turkey*, **19**, 65–78 (in Turkish, English abstract).

Özgül, N. (1984) Alanya Tectonic Window and geology of its western part. Ketin Symposium, 20–21 February 1984, Ankara, *Geological Society of Turkey*, 97–120 (in Turkish with English abstract).

Reynolds, R.C., Jr. (1985) *NEWMOD A Computer Program for the calculation of one-dimensional diffraction patterns of mixed-layered clays*. R.C. Reynolds, Jr., 8 Brook Rd., Hanover, New Hampshire, USA.

Robertson, A.H.F. (1994) Role of the tectonic facies concept in orogenic analysis and its application to Tethys in the Eastern Mediterranean region. *Earth Science Reviews*, **37**, 139–213.

Robertson, A.H.F. (2000) Mesozoic-Tertiary tectonic-sedimentary evolution of a south Tethyan oceanic basin and its margins in southern Turkey. Pp. 97–138 in: *Tectonics and Magmatism in Turkey and the Surrounding Area* (E. Bozkurt and J.A. Winchester, editors). Special Publication **173**, Geological Society, London.

Robertson, A.H.F. and Woodcock, N.H. (1981) Gödene Zone, Antalya Complex: volcanism and sedimentation along a Mesozoic continental margin, S.W. Turkey. *Geologische Rundschau*, **70**, 1177–1214.

Robinson, D. (1987) Transition from diagenesis to metamorphism in extensional and collision settings. *Geology*, **15**, 866–869.

Robinson, D. and Bevins, R.E. (1986) Incipient metamorphism in the Lower Palaeozoic marginal basin of Wales. *Journal of Metamorphic Geology*, **4**, 101–113.

Savin, S.M. and Epstein, S. (1970) The oxygen and hydrogen isotope geochemistry of clay minerals. *Geochimica et Cosmochimica Acta*, **34**, 25–42.

Savin, S.M. and Lee, M. (1988) Isotopic studies of phyllosilicates. Pp. 189–223 in: *Hydrous Phyllosilicates* (S.W. Bailey, editor). Reviews in Mineralogy, **19**, Mineralogical Society of America, Washington, D.C.

Şenel, M. (1997) *1:100,000 Scale Geological Maps of Turkey, Antalya M10, M11, L10, L11 and L12 quadrangles*. General Directorate of Mineral Research and Exploration, Ankara, Turkey.

Şenel, M., Dalkılıç, H., Gedik, İ., Serdaroğlu, M., Metin, S., Esentürk, K., Bölükbaşı, A.S., and Özgül, N. (1998) Orta Toroslar'da Güzelsu koridoru ve kuzeyinin stratigrafisi, Türkiye. *Bulletin of Mineral Research and Exploration of Turkey*, **120**, 171–198 (in Turkish).

Şengör, A.M.C. and Yılmaz, Y. (1981) Tethyan evolution of Turkey: a plate tectonic approach. *Tectonophysics*, **75**, 181–241.

Sheppard, S.M.F. and Gilg, H.A. (1996) Stable isotope geochemistry of clay minerals. *Clay Minerals*, **31**, 1–24.

Sheppard, S.M.F., Nielsen, R.L., and Taylor, H.P., Jr. (1969) Oxygen and hydrogen isotope ratios of clay minerals from porphyry copper deposits. *Economic Geology*, **64**, 755–777.

Sudo, T., Shimoda, S., Yotsumoto, H., and Aita, S. (1981) *Electron Micrographs of Clay Minerals*. Elsevier, Amsterdam, 203 pp.

Sun, S.S. and McDonough, W.E. (1989) Chemical and isotopic systematics of ocean basalts: Implications for mantle composition and processes. Pp. 313–345 in: *Magmatism in Ocean Basalts* (A.D. Saunders and M.J. Norry, editors). Special Publications, **42**, Geological Society, London.

Taylor, S.R. and McLennan, S.M. (1985) *The Continental*

Crust: Its Composition and Evolution. Blackwell, Oxford, UK, 312 pp.

Tekin, U.K. (2002) Lower Jurassic (Hettangian-Sinemurian) radiolarians from the Antalya Nappes, Central Taurids, Southern Turkey. *Micropaleontology*, **40**, 177–205.

Tekin, U.K. and Yurtsever T.S. (2003) Late Triassic (Early to Middle Norian) radiolarians from the Antalya Nappes, Antalya, SW Turkey. *Journal of Micropaleontology*, **22**, 147–162.

Ulu, Ü. (1983) Geological investigation in the Sugözü-Gazipaşa, Antalya. *Bulletin of Geological Engineering of Turkey*, **16**, 3–8 (in Turkish with English abstract).

Uysal, I.T. and Golding, S.D. (2003) Rare earth element fractionation in authigenic illite-smectite from Late Permian clastic rocks, Bowen Basin, Australia: implications for physico-chemical environments of fluids during illitization. *Chemical Geology*, **193**, 167–179.

Varol, E., Tekin, U.K., and Temel, A. (2007) Age and geochemistry of Middle to Late Carnian basalts from the Alakırçay Nappe (Antalya Nappes, SW Turkey): implications for the evolution of the southern branch of Neotethys. *Ofioliti*, **32**, 163–176.

Velde, B., Suzuki, T., and Nicot, E. (1986) Pressure-temperature-composition of illite/smectite mixed-layer minerals: Niger delta mudstones and other examples. *Clays and Clay Minerals*, **34**, 435–441.

Weaver, C.E. and Pollard, L.D. (1973) *The Chemistry of C1ay Minerals*. Developments in Sedimentology, **15**, Elsevier, Amsterdam, 213 pp.

Welton, E.J. (1984) *SEM Petrology Atlas*. American Association of Petroleum Geologists, Tulsa, Oklahoma, 237 pp.

Warr, L.N. and Rice, A.H.N. (1994) Interlaboratory standardization and calibration of clay mineral crystallinity and crystallite size data. *Journal of Metamorphic Geology*, **12**, 141–152.

Yılmaz, P.O. (1984) Fossil and K-Ar data for the age of the Antalya complex, SW Turkey. Pp. 335–347 in: *The Geological Evolution of the Eastern Mediterranean* (J.E. Dixon and A.H.F. Robertson, editors). Special Publications, **17**, Geological Society, London.

Zielinski, R.A. (1982) The mobility of uranium and other elements during alteration of rhyolite ash to montmorillonite: a case study in the Troublesome Formation, Colorado, U.S.A. *Chemical Geology*, **35**, 185–204.

(*Received 20 November 2009; revised 8 September 2010; Ms. 385; A.E. L.B. Williams*)